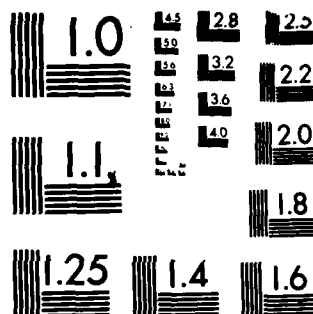MICROCOPY RESOLUTION TEST CHART

NATIONAL BUREAU OF STANDARDS-1963-A

AD-A142 206

AFGL-TR-84-0030

STUDY OF e-BEAM PROPAGATION IN THE
IONOSPHERE AND MAGNETOSPHERE

D.J. Strickland
H.W. Bloomberg
D.L. Lin

Science Applications, Inc.
Electromagnetic/Radiation Effects Division
1710 Goodridge Drive
McLean, Virginia   22102

Final Report
27 July 1979 – 31 December 1980

September 1983

DTIC
ELECTE
JUN 1 9 1984

A

This report has been reviewed by the ESD Public Affairs Office (PA) and is releasable to the National Technical Information Service (NTIS).

This technical report has been reviewed and is approved for publication

Charles W. Dubs

CHARLES W. DUBS
Contract Manager

Charles C. Pike

CHARLES P. PIKE, CHIEF
Spacecraft Interactions Branch

FOR THE COMMANDER

Rita C. Sagalyn

RITA C. SAGALYN, Director

SECURITY CLASSIFICATION OF THIS PAGE *(When Data Entered)*

REPORT DOCUMENTATION PAGE		READ INSTRUCTIONS BEFORE COMPLETING FORM
1. REPORT NUMBER AFGL-TR-84-0030	2. GOVT ACCESSION NO. *AD-A142-286*	3. RECIPIENT'S CATALOG NUMBER
4. TITLE *(and Subtitle)* STUDY OF e-BEAM PROPAGATION IN THE IONOSPHERE AND MAGNETOSPHERE		5. TYPE OF REPORT & PERIOD COVERED FINAL REPORT 27 July 79 - 31 December 80
		6. PERFORMING ORG. REPORT NUMBER SAI-102-83-07
7. AUTHOR(s) D. J. Strickland, H. W. Bloomberg, and D. L. Lin		8. CONTRACT OR GRANT NUMBER(s) F19628-79-C-0125
9. PERFORMING ORGANIZATION NAME AND ADDRESS SCIENCE APPLICATIONS, INC. Electromagnetics/Radiation Effects Division 1710 Goodridge Drive, McLean, Virginia 22102		10. PROGRAM ELEMENT, PROJECT, TASK AREA & WORK UNIT NUMBERS 62101F 760115AB
11. CONTROLLING OFFICE NAME AND ADDRESS Air Force Geophysics Laboratory Hanscom AFB, Massachusetts 01731 Monitor/Charles Dubs/PHK		12. REPORT DATE September 1983
		13. NUMBER OF PAGES 70
14. MONITORING AGENCY NAME & ADDRESS(*If different from Controlling Office*)		15. SECURITY CLASS. *(of this report)* UNCLASSIFIED
		15a. DECLASSIFICATION/DOWNGRADING SCHEDULE

16. DISTRIBUTION STATEMENT *(of this Report)*

Approved for public release; distribution unlimited.

17. DISTRIBUTION STATEMENT *(of the abstract entered in Block 20, if different from Report)*

18. SUPPLEMENTARY NOTES

19. KEY WORDS *(Continue on reverse side if necessary and identify by block number)*

electron beams, ionosphere, electron transport, plasma turbulence,
rocket fired beams

20. ABSTRACT *(Continue on reverse side if necessary and identify by block number)*

A two-dimensional (r,E) Monte Carlo electron transport model has been developed
to study the energy deposition and spreading of kilovolt electron beams in the
ionosphere. MCBE is the name of the computer code incorporating the model.
The beam electrons scatter and lose energy through particle-particle interactions.
These processes are treated by applying the Goudsmit-Saunder multiple scattering
formula and assuming energy loss is continuous. Results have been obtained
for several beam energies and some have been compared to the results of Berger,
et al. (1970). We obtain excellent agreement in the altitude profile of energy

DD $_{1\ JAN\ 73}^{FORM}$ 1473   EDITION OF 1 NOV 65 IS OBSOLETE

SECURITY CLASSIFICATION OF THIS PAGE *(When Data Entered)*

ABSTRACT *(Continued):*

deposition, but poor agreement in spreading. We find there to be less spreading along with a weaker dependence of this spreading on the starting beam electron energy. An analytic model has been developed to test the numerical results and contains the magnitude and weak dependence on beam energy of the observed spreading. This model has now been published with a copy of the reprint appearing at the end of this report. Another aspect of the work has been to investigate the effect of plasma turbulence on beam propagation. Time did not permit the development of an actual model to be incorporated into the MCBE formulation. Our efforts instead have been directed to a study of the expected turbulence which is discussed throughout the text. Finally, a survey of rocket e-beam experiments and associated theoretical investigations was conducted which has been documented in Section 1 of this report. The survey is current as of late 1980 and reports on all experiments known to us at that time. Several tables are included which summarize various aspects of the experiments, as well as a bibliography subdivided by experiment.

TABLE OF CONTENTS

Section 1

INTRODUCTION AND SUMMARY

This is the final report on Contract Number F19628-79-C-0125 titled *"Electron Beam Propagation in the Ionosphere"*. During this contract, we have:

(1) carried out a fairly thorough literature survey on rocket electron (e) beam experiments and theoretical investigations dealing with beam-plasma interactions;

(2) developed a 2-D Monte Carlo electron transport code;

(3) applied the code to beam energy deposition and spreading; and

(4) made recommendations with regard to future experiments.

The motivation behind these efforts is an Air Force Geophysics Laboratory program designed to fire kilovolt ion and electron beams from rockets and possibly the space shuttle.

The highlight of the work performed was the development and application of code MCBE which is the code referred to above. This code solves the equation of motion for some large number of electrons in the presence of an exponentially varying neutral atmosphere and geometric field. Along the electron's path of motion, energy is allowed to be deposited continuously. Frequent changes in the electrons' guiding center take place through scattering which is modeled by use of the Goudsmit-Saunderson multiple scattering formula.

The Monte Carlo nature of MCBE comes from scattering
treatment and in some cases from sampling distribution functions
defining the initial beam conditions. The quantities calculated
are:

> (1) the r,z distributions of energy and charge
>   deposition;
>
> (2) the 1-D distributions of energy deposition
>   in either r or z obtained by integrating over
>   the other spatial dimension; and
>
> (3) detailed radial and time information on those
>   electrons which have backscattered through
>   the incident plane.

The current description of electron interactions in MCBE
does not include wave-particle effects.

A noteworthy result obtained from various runs
of MCBE is the insensitivity of the spreading to the starting
energy of the beam electrons. This contrasts with the results
of Berger, et al.[24] (see the appendix for further details)
and leads to differences on the order of three in mean radius
of energy deposition for a starting energy of 20 keV. Because
of this disagreement, an analytic model of guiding center
diffusion was developed to test the MCBE results. The model
confirms both the insensitivity of spreading to the starting
beam electron energy and the magnitude of the spreading.
This work has been published with a copy of the reprint appearing
in the appendix.

An application of MCBE and the above analytic
model has been made to interpret the observed optical
streak widths produced by ECHO-4 beams emitted downward into
the E-region. The calculated widths give reasonable agreement
with the observations for some streaks and significantly

underestimate the observations for others. Generally, beam
spread increased for those beams fired near-rocket apogee.
This suggests that the differences can be attributed to plasma
turbulence effects occurring in regions of lower collision
frequency. The comparisons quantify the amount of the beam
spreading due to the turbulence.

Each of the chapters to follow was originally written
as a self-contained document. Section 2 comes from an interim
report which documents our literature search. Section 3
comes from combined Quarterly Reports 2 and 3 and presents
MCBE results and relates them to ECHO-4 data. A discussion
is included of the rate of plasma turbulence in the spreading
of the emitted beams. Section 4 contains a memo submitted
during the contract period providing suggestions for future
rocket fixed beams experiments. Finally, the appendix contains
a copy of a JGR paper based on part of the contract work.
The paper describes the analytic model for beam spreading
referred to above.

Section 2

A REVIEW OF ROCKET e-BEAM EXPERIMENTS
AND ASSOCIATED THEORETICAL INVESTIGATIONS

2.1 INTRODUCTION

Since the first rocket experiment with injection
of e-beams into the ionosphere by Hess et al.[1], nearly
two dozen such experiments have been conducted, providing
an impressive body of information on e-beam propagation
in the ionosphere and magnetosphere. This information has
come from combinations of on-board, separated nose cose,
and ground based measurements of particles, optical emissions,
and rf emissions. Much has been learned about the interaction
of e-beams with the neutral particles and plasma within
the propagating region, but such experiments have also left
a number of questions directly related to beam-plasma inter-
actions unanswered.

We will attempt in this report sponsored by the
Air Force Systems Command under Contract Number
F19628-79-C-0125, to provide a fairly comprehensive review
of the above subject, noting, by experiment, parameters
of interest and those observed phenomena which are not cur-
rently well understood.

2.2 ROCKET e-BEAM EXPERIMENTS

2.2.1 Overview

To date (late 1979) we are aware of fifteen rocket e-beam
experiments that have been conducted in the ionosphere.
These are two early experiment reported by Hess et al.[1],
Davis et al.[2], and Davis[3], four experiments labeled

2-1

ECHO I-ECHO IV, the Russian experiments ZARNITSA 1-2, the Franco-Russian experiment ARAKS, five experiments in the PRECEDE-EXCEDE program, and a Norwegian experiment[a]. In addition, Cohen et al.[5] have conducted an important experiment where a rocket fired ion beam (in conjunction with an electron beam) was used to study the effects of beam emission on spacecraft charging. Since characterization of beam propagation was not a primary goal of the experiment, it has not been considered in this review. The value of beam propagation experiments lies in their potential to obtain information on such subjects as:

- the geomagnetic field:
  - -- conjugate point locations,
  - -- field line lengths,
  - -- magnetospheric field configuration (e.g., transition from closed to open field lines);

- drift rates:
  - -- curvature,
  - -- gradient,
  - -- $E \times B$,

- particle-particle interactions:
  - -- transport properties such as scattering and penetration depths,
  - -- neutral densities,
  - -- cross sections,
  - -- rate coefficients;

- wave-particle interactions.

The fundamental problem of e-beam propagation comes under the last two headings and addresses how particle-particle and wave-particle interactions modify the beam's

---

a) Recently, Winckler[4] has written a report which expands this list by including the Russian "Feyerwerk" experiment, 5 experiments in the Japan "K" rocket series, and 2 $E_{||}B$ experiments with rockets fired from the Churchill Research Range. Information on the experiments is not now available in the open literature, and they have not been considered in this report.

lateral extent and its distributions in energy and pitch
angle. Prior to the first e-beam experiment in the iono-
sphere (Hess et al.[1]), it was an open question as to whether
a beam would even propagate an appreciable distance before
some plasma instability led to its destruction. Experiment
has shown that, indeed, beams do propagate and seem to retain
much of their character over great distances such as traversed
in an "echo" from the conjugate point. Experiment has also
shown that mechanisms are operating on the beam, presumably
of the collective or wave-particle type which lead to effects
poorly understood at this time. Examples are anomalous
backscatter, high frequency rf generation, and anomalous
diffuseness of artificial auroral streaks.

In the sub-sections to follow, we will be addressin
the above-mentioned experiments by way of presenting launch
information, beam parameter values, diagnostics, and unexplaineu
effects. We do wish to caution the reader that our information
comes from published literature and is not necessarily complete.
An example of this might be pulse durations where in fact,
the values given may be part of a larger set not discussed
in its entirety in the literature. We believe, however,
that sufficient information will follow to provide the reader
with a good picture of rocket e-beam experiments and what
is and is not understood about them to date.

2.2.2   Parameters and Instrumentation

An attempt has been made by us to characterize
the various experiments in the form of tables giving a variety
of paramaters and instruments which recorded data of a general
interest to this program. The reader will find, however,
a number of blank spaces in these tables, especially for
instrumentation. This simply means that we have not found
the given information in the literature base used for this
review. An advantage of the format presentation chosen,

in spite of this, is that newly acquired information may
be easily added which we intend to do as this program continues.

Table 1 provides a list of the experiments along
with basic information such as launch date, launch site,
and rocket apogee. We see that the experiments cover a
time span of one decade and latitude range from mid to high
latitude. This latter fact is worth noting since environmental
conditions, in terms of beam-plasma interactions, may vary
significantly from the mid-latitude ionosphere to the auroral
ionosphere where natural streams of energetic electrons
are frequently present.

The parameters we have chosen to characterize
the beam are energy, current, power, pulse duration, and
injection angle. An example of how some of these parameters
have been programmed into an experiment (ECHO IV) is provided
in Figure 1. We observe a range of pulse widths and injection
pitch angles which is not atypical for rocket e-beam experi-
ments. More information is given in Table 2 where we have
attempted to specify the above parameters by experiment.
We wish to stress that the parameter values shown may be
parts of larger sets. We believe, however, that most entries
do cover the experimental range. The convention chosen
on pitch angle is that 0° corresponds to the downward direction.

The basic types of recording devices used in the
experiments were:

- particle detectors,
- photometers,
- photo-spectrometers,
- rf receivers,
- radar systems, and
- TV systems.

TABLE 1. ROCKET e-BEAM EXPERIMENTS — LAUNCH AND TRAJECTORY PARAMETERS

EXPERIMENT	LAUNCH DATE	LAUNCH SITE	L PARAMETER	APOGEE (km)	Kp
HESS ET AL	Jan. '69	Wallops Is., Va.	2.6	296	
DAVIS		Kauai, Hawaii			
ECHO I	Aug. '70	Wallops Is., Va.	2.6	350	1+
ECHO II	Sept. '72	Ft. Churchill, Manatoba	∿8.8		
ECHO III	Apr. '74	Poker Flat, Alaska	6	278	1
ECHO IV	Jan. '76	Poker Flat, Alaska	6	215	
ZARNITSA-I					
ZARNITSA-II				155	
ARAKS	Jan. '75	Kerguelen Island			
(2 experiments)	Feb. '75	(49° S)			
PRECEDE	Oct. '74	White Sands, N. M.	∿2	120	
EXCEDE-II TEST	Apr. '75	Poker Flat, Alaska	6	135	
EXCEDE-SWIR	Feb. '76	Poker Flat, Alaska	6	99	
PRECEDE-II	Dec. '77	White Sands, N. M.	∿2	102	
EXCEDE-SPECTRA	Oct. '79	Poker Flat, Alaska	6	130	
NORWEGIAN EXPERIMENT					
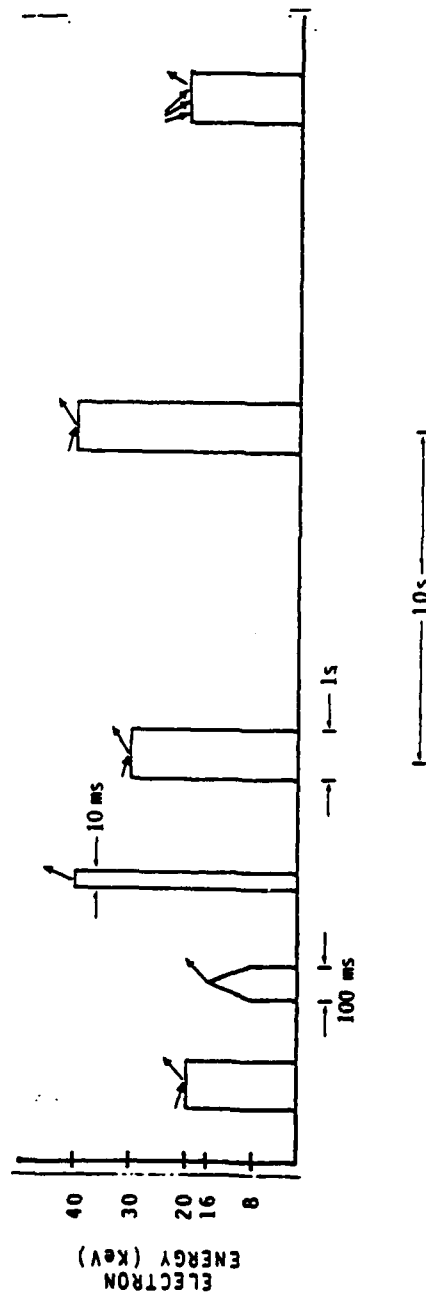
FIGURE 1. ECHO IV Gun Sequence

Shown is a sequence of four "marker" pulses. Single "picket" and "spike" pulses are shown. Between marker pulses are 18 such pickets and 18 such spikes. Arrows above pulses indicate pitch angle of electrons with respect to a vertical magnetic field. Multiple arrows show time variation of pitch angle within pulse.

TABLE 2. ROCKET e-BEAM EXPERIMENTS — BEAM PARAMETERS

EXPERIMENT	MAX. POWER (kW)	PULSE DURATION (ms)	BEAM ENERGY (keV)	BEAM CURRENT (mA)	INJECTION ANGLES (DEGREES)
HESS ET AL	5	≤1000	≤10	≤500	
DAVIS					
ECHO I	3	16	35–43	70	68–112
ECHO II	3.8	64	4–47	80	~0–180
ECHO III		2,8,32	32–37		
ECHO IV	2.5	1000	16–38	70	70,110,30–150 (sweep-mode)
ZARNITSA-I					
ZARNITSA-II	4.5	400	7,9	300–500	30–90
ARAKS	13.5	20,1280, 2560	15,27	<500	0,70,140
PRECEDE	2		2.5	800	140–180
EXCEDE-II TEST	30	~1000			
EXCEDE-SWIR	3		3	1000	
PRECEDE-II	20	4300	3	7000	
EXCEDE-SPECTRA					
NORWEGIAN EXPERIMENT					

In a given experiment, some of these would be located on the ground around the launch site, on the payload, and possibly on the ground below the conjugate point. Table 3 provides a list of instruments by experiment and places them into either an on-board or ground-based category.

Several types of particle detectors are noted in the table. Most of these were used to measure the return of beam particles due to mirroring and scattering (by particle-particle and wave-particle interactions). Most of the effort which went into the ECHO experiments was directed to this type of measurement. The retarding potential analyzer (RPA), however, was used to measure the return current (low energy) needed to keep the electron-guns functioning. On all experiments, attention was given to vehicle potential and its variation with time.

RF recievers were used to record signals generated by the beam interacting with the plasma. In some cases, these receivers were well positioned by being located in ejected nose cones (e.g., on ECHO I, ECHO II, and ARAKS). For those cases, rf signals able to propagate in the plasma environment of the ionosphere could be detected. Observations of ground based rf signals have been more limited, but radio signal signatures from beam injection experiments have been obtained.

The remaining instrumentation appearing in Table 3 needs litte explanation. Radar systems were used to track the rocket (not relevant to this discussion) and measure ionization produced by beam energy degradation in the lower ionosphere (e.g., in the ARAKS experiment). Photometers, usually recording N_2^+ 3914A and OI 5577A emission, provided a measure of how much energy was being deposited when the beam produced an artificial auroral streak. Photo-spectrometers give the strengths of many optical features which may be used to better understand chemical processes. This,

TABLE 3   ROCKET e-BEAM EXPERIMENTS—INSTRUMENTATION

EXPERIMENT	ON-BOARD	GROUND-BASED
HESS ET AL	Retarding Potential Analyser (RPA) (0–2 keV)	TV, Radar, RF, Photometers
DAVIS		TV
ECHO-I	RF (in ejected nose cone) Particle (scintillation, solid state)	
ECHO-II	RF (in ejected nose cone), Particle (electrostatic (.9–45 keV), solid state) Proportional (for Bremsstrahlung)	
ECHO-III	Particle (electrostatic, scintillation) Photometer (3914A)	
ECHO IV	Particle (unspecified), Photometers (3914A & 5577A)	TV
ZARNITSA-I	Particle (electrostatic 1–14 keV), Magnetometer, Radar Transponder	TV, Radar, RF(300Hz–15KHz)
ZARNITSA-II		TV, Radar, RF (22.5–80MHz)
ARAKS	Particle, RF (in ejected nose cone)	Radar (conjugate point) RF (10–75 MHz)
PRECEDE	RPA	TV, Photometers (3914A & 5577A) Spectograph (4200–8500A)
EXCEDE-II TEST	RPA, Photometers (3914A & 5577A), Radiometers (2.7 & 4.3 μm)	TV, Photometers (3914A & 5577A)
EXCEDE-SWIR	22 Photometers, Radiometer, Ion Mass Spectrometer	TV, Photometers (3914A & 5577A)
PRECEDE-II	IR Interferometer	TV, Photometers (3914A & 5577A) UV & Visible Spectrographs
EXCEDE-SPECTRA		

in fact, has been the emphasis in the PRECEDE-EXCEDE program with particular attention directed to chemistry affecting IR emission. Finally, TV systems have been employed to search for auroral streaks produced by either downward injection, upward injection from low in the ionosphere, or upward injection at higher altitudes leading to an echo. Streaks have been recorded on many of the experiments starting with the first one reported by Hess et al.[1] In none of the experiments, however, have streaks been recorded for beam energy deposition following an echo.

2.2.3   Observations

Based on the literature base we have developed to this point, the experiments of most interest to this program are ECHO I - IV, ZARNITSA-2 and ARAKS. Taken as a whole, these experiments (as well as the first by Hess) have significantly advanced our understanding of e-beam propagation in the ionosphere and magnetosphere. They have also obtained several results which cannot be explained by classical theory. We wish to point out such results in this section and to do so we have constructed Table 4. Here, we have divided the observations into the categories of particle, rf, and optical for six experiments noted above. Blank spaces mean either the absence of that particular measurement or the absence of information in the literature. In some places we have noted the measurement even if it produced no surprises. Our emphasis here, however, is on measurements which imply strong beam-plasma interactions and thus in turn are not well understood. Prior to their discussion, however, we note that particle measurements such as those on ECHO IV show that the beam can remain reasonably well confined over large propagation distances such as traversed in an echo from the conjugate region. These imply that beam-plasma interactions are not particularly destructive to the beam. There is reason to believe,

Table 4. ROCKET e-BEAM EXPERIMENTS - OBSERVATION HIGHLIGHTS

EXPERIMENT	PARTICLES — ENERGETIC PARTICLES FROM BELOW (SCATTERING AND MIRRORING)	PARTICLES — ENERGETIC PARTICLES FROM ABOVE (LOCAL SCATTERING)	PARTICLES — ENERGETIC PARTICLES FROM ABOVE ((ECHOS) SCATTERING AND MIRRORING)	RF	OPTICAL — IMAGING	OPTICAL — NON-IMAGING SPECTRAL
ECHO I	Amount of backscatter as classically predicted	Greatly enhanced above classically predicted value	Echos observed. Enhanced drift displacements and long echo delays. Fluxes much smaller than classically predicted. Some double echos (long delay for second signal)	Signals observed in ejected nose cone antenna: plasma frequency mode observed at 6.5 MHz; electron cyclotron harmonic (2nd) observed at 2.5 MHz; lower hybrid resonance observed at 1 MHz; whistler mode observed at 8 KHz. Strong increase in plasma frequency and whistler mode radiation for θ_I >100°.		
ECHO II	Spectra observed and reported (~0 - 45 keV) Amount of backscatter as classically predicted	See ECHO I. Spectra observed (strongly degraded)	Uncertain that signals are from echos	Same modes observed as in ECHO I. Strong whistler mode emission observed in wide frequency band detector.		
ECHO III			Echos observed. Increase in bounce times from one pulse to next not understood			One echo produced observable on-board 3914A signal
ECHO IV			Echos observed. Bounce times and drift displacements as predicted. Beams showed small lateral spreading.	G.B.* measurements near second electron cyclotron harmonic (2.96 MHz)	TV observed streaks (10). Diffuse streaks observed during time when rocket was near apogee (215 km)	One echo produced observable on-board 3914A signal
ZARNITSA-2				G.B.* measurements at several locations around launch site (22.5 - 80 MHz). Strongest signals obtained with 27-50 MHz spectrograph and radar at 22.5 and 33.8 MHz. Spectrograph data allow for θ_I and a dependences. Radar observed halo around rocket. Near apogee, radar signal due to combination of halo and artificial auroral streak.	TV observed halo around rocket and artificial auroral streaks below (halo and streaks resolvable). Several percent of beam power needed to produce halo	
ARAKS	Amount of backscatter as classically predicted	Greatly enhanced above classically predicted value		G.B.* measurements at 10, 15, 25, 50, and 75 MHz around launch site as functions of θ_I and a. G.B. radar at conjugate point detected beam ionization. Unexplained delays in onset of radar signature.		G.B.* spectrometer recorded the many well known lines appearing in auroras. Fairly intense continuum also observed (5500 - 7000A) when rocket was below 140 km.

* G.B. - Ground based   * θ_I - beam injection angle

however, that the strength of the interaction can vary significantly depending on the specific properties of the propagation medium and particularly on the position of beam injection.

A feature requiring the presence of a rather strong beam-plasma interaction is backscatter from just above the rocket as observed on ECHO I and II and on ARAKS. The measured signals were orders of magnitude above that predicted for particle-particle scattering. Another such feature is the halo of strong enhanced ionization (not accounted for by injected plasma sources) in the rocket environment as observed on the ZARNITSA and ARAKS experiments. The halos were detected by high frequency rf signals propagating from the vicinity of the rockets and by ground based radar and TV systems. In the ZARNITSA 2 experiment, it was suggested that several percent of the initial beam energy became converted to plasma potential and kinetic energy in the local environment of the rocket. A number of other observations can be cited supporting significant beam-plasma interactions. Diffuse auroral streaks were observed on ECHO IV when the beam originated near apogee (215 km). Unexpected delays in echos were observed on ECHO I and III. In the ARAKS experiment long delays in the onset of radar return signals from regions of beam deposition at the conjugate point were observed. In some instances of ECHO I injection there were observed pairs of echos with the first arriving at about the predicted time while the second arrived much later but too soon to be from a second conjugate bounce.

In addition to observations that show beam dissipation, rf signals have been observed to result from beam-plasma interactions which largely maintain the integrity of the beam. These signals, although not now well understood, could prove to be valuable diagnostics on the characteristics of the propagating beam. The frequencies of these signals are in the MHz range corresponding to ambient plasma frequencies as well as electron cyclotron harmonics and in the sub-MHZ range corresponding to whistler modes.

2.2.4   Bibliography by Experiment

HESS et al.

1.   Hess, W. N., M. C. Trichel, T. N. Davis, W. C. Beggs,
      G. E. Kraft, E. Stassinopoulos, and E. J. R. Maier,
      "Artificial Auroral Experiment: Experiment and Principal
      Results," J. Geophys. Res., 76, 6067-6081, 1971.

2.   Davis, T. N., T. J. Hallinan, G. D. Mead, J. M. Mead,
      M. C. Tichel, and W. N. Hess, "Artificial Auroral Experi-
      ment: Ground-based Optical Observations," J. Geophys.
      Res., 76, 6082-6092, 1971.

DAVIS

1.   Davis, T. N., "Television Observations of Artificial
      Aurora and Analyses of Flight Data from NASA Payload,"
      12.18 NE, final report, NASA Contract NAS9-11815, Geophys.
      Inst., Fairbanks, Alaska, October 1974.

2.   Davis, T. N., "Optical Observations of Active Experiments,
      paper presented at the ARAKS Symposium, Franco-Soviet
      Symposium on Active Experiments in the Magnetosphere,"
      Toulouse, France, May 9-14, 1976.

ECHO

1.   Hendrickson, R. A., R. W. McEntire, and J. R. Winckler,
      "Electron Echo Experiment: A New Magnetospheric Probe,"
      Nature, 230, 564, 1971.

2.   Jones, T. W. and P. J. Kellogg, "Plasma Waves Artifically
      Induced in the Ionosphere," J. Geophys. Res., 78, 2166-
      2175, 1973.

3.   Cartwright, D. G and P. J. Kellogg, "Observations of
      Radiation from an Electron Beam Artificially Injected
      into the Ionosphere," J. Geophys. Res. 79, 1439, 1974.

4.   McEntire, R. W., R. A. Hendrickson, and J. R. Winckler,
      "Electron Echo Experiment 1: Comparison of Observed
      and Theoretical Motion of Artificially Injected Electrons
      in the Magnetosphere," J. Geophys. Res. 79, 2343, 1974.

5.   Hendrickson, R. A., R. W. McEntire, and J. R. Winckler,
      "Echo 1: An Experimental Analysis of Local Effects
      and Conjugate Return Echos from an Electron Beam Injected
      into the Magnetosphere by a Sounding Rocket," Planet.
      Space Sci. 23, 1431, 1975.

6. Winckler, J. R., "An Investigation of Wave-Particle Interactions and Particle Dynamics Using Electron Beams Injected from Sounding Rockets," Space Sci. Rev. 15, 751, 1974.

7. Winckler, J. R., R. A. Arnoldy, and R. A. Hendrickson, "Echo II: A Study of Electron Beams Injected into the High-Latitude Ionosphere from a Large Sounding Rocket," J. Geophys. Res. 80, 2083, 1975.

8. Israelson, G. A. and J. R. Winckler, "Measurements of 3924A Light Production and Electron Scattering from Electron Beams Artificially Injected into the Ionosphere," J. Geophys. Res. 80, 3079, 1975.

9. Arnoldy, R. L., R. A. Hendrickson, and J. R. Winckler, "A Determination of F Region Effective Recombination Coefficients from the Echo 2 Sounding Rocket Plasma Wave and Particle Measurements," J. Geophys. Res. 80, 4307-4312, 1975.

10. Hendrickson, R. A., J. R. Winckler, and R. L. Arnoldy, "Echo III: The Study of Electric and Magnetic Fields with Conjugate Echos from Artificial Electron Beams Injected into the Auroral Ionosphere," Geophys. Res. Lett. 3, 409, 1976.

11. Monson, S. J., P. J. Kellogg, and D. G. Cartwright, "Whistler: Mode Plasma Waves Observed on Electron Echo 2," J. Geophys. Res. 81, 2193-2199, 1976.

12. Monson, S. J. and P. J. Kellogg, "Ground Observations of Waves at 2.96 MHz Generated by an 8- to 40-KeV Electron Beam in the Ionosphere," J. Geophys. Res. 83, 121-131, 1978.

13. Hallinan, T. J., H. C. Stenback-Nielson, and J. R. Winckler, "The Echo 4 Electron Beam Experiment: Television Observation of Artificial Auroral Streaks Indicatin Strong Beam Interactions in the High-Latitude Magnetosphere," J. Geophys. Res. 83, 3263, 1978.

ZARNITSA-1

1. Cambou, F., U. S. Dokoukine, V. N. Ivchenko, G. G. Managadze, V. V. Migulin, O. K. Nazarenko, A. T. Nesmyanovitch, A. Kh. Pyatsi, R. Z. Sagdeev, and I. A. Zhulin, "The Zarnitza Rocket Experiment of Electron Injection," Space Research, 15, Akademic-Verlag, Berlin, 491, 1975.

ZARNITSA-2

1.   Mishin, E. V. and Yu. Ya. Ruzhin, "Beam-Plasma Discharge
     During Electron Beam Injection in Ionosphere; Dynamics
     of the Region in Rocket Environment in ARAKS and
     ZARNITSA-2 Experiments," Preprint No. 21a, Institute
     of Terrestial Magnetism, Ionosphere and Radiowave Propa-
     gation, Moscow, 1978.

ARAKS

1.   Cambou, F., J. Lavergnat, V. V. Migulin, A. I. Morozov,
     B. E. Paton, R. Pellat, A. Kh. Pyatsi, H. Reme,
     R. Z. Sagdeev, W. R. Sheldon, and I. A. Zhulin,
     "ARAKS-Controlled or Puzzling Experiment?," Nature,
     271, 723-726, 1978.

2.   Mishin, E. V. and Yu. Ya. Ruzhin, "Beam-Plasma Discharge
     During Electron Beam Injection in Ionosphere; Dynamics
     of the Region in Rocket Environment in ARAKS and ZARNITSA-2
     Experiments," Preprint No. 21a, Institute of Terrestial
     Magnetism, Ionosphere and Radiowave Propagation, Moscow,
     1978.

PRECEDE

1.   O'Neil, R. R., F. Bien, D. Burt, J. A. Sandock, and
     A. T. Stair, Jr., " Summarized Results of the Artificial
     Auroral Experiment, Precede," J. Geophys. Res. 83,
     3273-3280, 1978.

2.   O'Neil, R. R., ed., "PRECEDE II: Summarized Results
     of an Artificial Auroral Experiment," AFGL-TR-78-0063,
     Air Force Geophysics Laboratory, Hanscom AFB, Mass.,
     1978, AD A061717.

3.   O'Neil, R. R., E. T. P. Lee, and E. R. Huppi, "Auroral
     O('S) Production and Loss Processes: Ground-Based
     Measurements of the Artificial Auroral Experiment Precede,"
     J. Geophys. Res. 84, 823-833, 1979.

EXCEDE

1.   O'Neil, R. R., E. T. P. Lee, A. T. Stair, Jr., J. C.
     Ulwick, "EXCEDE II," AFGL-TR-76-0308, Air Fordce Geophysics
     Laboratory, Hanscom AFB, Mass., 1976.

2.   O'Neil, R. R., O. Shepherd, W. P. Reidy, J. W. Carpenter,
     T. N. Davis, D. Newell, T. C. Ulwick, and A. T. Stair,
     Jr., "EXCEDE II Test, An Artificial Auroral Experiment:
     Ground-Based Optical Measurements," J. Geophys. Res.
     83, 3281-3288, 1978.

2.3   COLLECTIVE EFFECTS

2.3.1   Overview

By collective effects we mean the totality of
fluctuations in a plasma with which a rocket fired beam may
interact to result in processes different than or substantially
enhanced from usual particle-particle interactions. Since
the ambient properties of the ionosphere and magnetosphere
can be determined reasonably well, it has been possible
to anticipate the results of particle-particle interactions
as well as the classical drift character of the individual
beam-particles within inhomogeneous magnetic fields. It
is the complex array of unanticipated results which have
occurred in rocket fired beam experiments that has given
rise to an intense interest in collective effects.

In the study of these effects it is useful to
consider three different regions of space. The first is
the region close to the beam injector where potential build-
up between various rocket components is possible. Such
configurations can lead to important return current effects,
which often can be enhanced by the presence of rocket gases
remaining in the vicinity of the gun. Not only is it difficult
to characterize the environment of the gun but it can be
expected that disruptive beam-particle interactions will
occur near the injection position. The major phenomenon
observed near the rocket is an enhancement of the ambient
electron density in an effect known as the beam plasma discharge
(BPD). The second region of interest is the ionosphere
at some distance from the rocket. Here the ambient environment
is often times sufficiently free of fluctuations that we
can confidently associate collective effects with fluctuations
induced by the beam-plasma interaction. The effects of
beam interaction within the ionosphere have been monitored
through nose cone antennas which receive rf signals. Among
suspected collective effects have been the appearance of

diffuse artificial aurora streaks as well as enhanced local
backscatter with either upward or downward injection. The
third region of interest is the magnetosphere through which
the beam propagates in experiments involving echos or artificial
aurora created at the conjugate point. Collective fluctuations
in this region may be caused by instability induced through
natural phenomena as well as through beam-plasma interaction.
The major observation of collective effects in this region
involve echo delays as well as large degradations in the
expected flux of mirroring particles.

In Section 2.3.2 we examine the important parameter
regimes in space. The importance in differentiating between
absolute and convective instabilities in finite width beam
experiments is discussed in Section 2.3.3. Classification
of the rf signals received by antennas with respect to plasma
modes is made in Section 2.3.4. Finally, in Section 2.3.5
we discuss possible mechanisms to explain the experimental
results apparently involving collective effects. Unfortunately,
no concensus seems to exist as to the cause of the major
collective phenomena. This points up the importance not
only of increasing the emphasis on theoretical studies but
also in the design of more controlled experiments in the
future.

2.3.2   Parameter Regimes

When one considers the nature of beam-plasma
collective effects that can arise in experiments involving
beams fired from rockets, it is important to keep in mind
the wide range of parameter regimes that are encountered.
Beams are generally ejected from rockets between the E and
F regions. Table 5 indicates the neutral and electron number
densities at the various heights when beams are injected.
At low injection altitudes, the neutral particle density
may be so large that a very high neutral-electron collision
frequency may be thought to preclude any collective effects.

TABLE 5. TYPICAL IONOSPHERIC PARAMETERS AS FUNCTIONS OF HEIGHT (L=2.56)
NUMBERS WITHIN PARENTHESES INDICATE POWER OF TEN FOR MULTIPLICATIVE FACTOR

Height (Km)	75	80	90	100	110	120	130	140	150	175	200	250
B (gauss)	.50	.50	.50	.50	.50	.49	.49	.49	.49	.48	.48	.46
n_e (cm^{-3}) day	1(2)	1(3)	8(3)	1(5)	1(5)	1.5(5)	2(5)	3(5)	3(5)	3(5)	4(5)	8(5)
n_e (cm^{-3}) night	0	10	60	1(3)	2(3)	2(3)	2(3)	2(3)	2(3)	2(3)	3(3)	
n_n (cm^{-3})	1(15)	4(14)	4(13)	1(13)	2(12)	8(11)	3(11)	1(11)	5(10)	2(10)	8(9)	3(9)
ω_{pe} ($\frac{rad}{sec}$) (day)	5.6(5)	1.8(6)	5(6)	1.8(7)	1.8(7)	1.8(7)	2.5(7)	3.1(7)	3.1(7)	3.1(7)	3.6(7)	5(7)
ω_{ce} ($\frac{rad}{sec}$)	8.88(6)	8.86(6)	8.82(6)	8.77(6)	8.73(6)	8.69(6)	8.65(6)	8.60(6)	8.56(6)	8.46(6)	8.35(6)	8.15(6)
ω_{pe}/ω_{ce}	.063	.20	.57	2.05	2.06	2.07	2.89	3.60	3.62	3.67	4.31	6.13

TABLE 5. TYPICAL IONOSPHERIC PARAMETERS AS FUNCTIONS OF HEIGHT (L=2.56)
NUMBERS WITHIN PARENTHESES INDICATE POWER OF TEN FOR MULTIPLICATIVE FACTOR

(Continued)

Height (km)	300	350	400	500	750	1,000	2,000	4,000	6,000	8,000	9,938
B (gauss)	.45	.44	.43	.41	.37	.33	.22	.11	.056	.032	.019
n_e (cm^{-3}) day	8(5)	7(5)	6(5)	2(5)	5(4)	1.7(4)	4(3)	1(3)			
n_n (cm^{-3})	8(8)	5(8)	1(8)	4(7)							
$\omega_{pe}\left(\frac{rad}{sec}\right)$ (day)	5.(7)	4.7(7)	4.4(7)	2.5(7)	1.3(7)	7.4(6)	3.6(6)	1.8(6)			
$\omega_{ce}\left(\frac{rad}{sec}\right)$	7.96(6)	7.77(6)	7.58(6)	7.23(6)	6.44(6)	5.76(6)	3.79(6)	1.84(6)	9.8(5)	5.6(5)	3.27(5)
ω_{pe}/ω_{ce}	6.28	6.05	5.80	3.46	2.02	1.28	.95	.98			

This can be misleading, however. Even though the high collision frequency may serve to prevent the growth of large amplitude waves (ignoring for the moment resistive instability), still, self-electric field effects can be important, since the background plasma density decreases for lowering altitudes beneath the E-layer. The usual test for the importance of the self-electric field is to compare the beam density with the ambient plasma density. The radius of the beam in the vicinity of the rockets can usually be assumed to be or order of the Larmor radius:

$$\rho = \frac{V_\perp}{\omega_{ce}} = \frac{V\sin\theta}{\omega_{ce}} \qquad (1)$$

where V is the speed of an injected beam particle, θ is the pitch angle, and ω_{ce} is the electron gyro-frequency. Since for the non-relativistic particle beams of usual interest the speed is related to the energy by :

$$V = \sqrt{\frac{2E}{M}}$$

where M is the electron mass, and since the beam number density is related to the total current by:

$$N_b eV\cos\theta \cdot \pi\rho^2 = I \qquad\qquad ,$$

we can finally express N_b in terms of the usual parameters associated with the experiment as well as with the ambient environment:

$$N_b = \frac{IeB^2}{\pi c^2 (2E)^{3/2} \sqrt{M}\cos\theta \sin^2\theta} \qquad (2)$$

Equation (2) shows that for the practical case of small pitch angle N_b will be larger than the ambient plasma density. In this case the ambient plasma cannot charge neutralize the beam so that the electrostatic repulsion should be included.

Gendrin[6] and Alekkin et al.[7] have examine the radial
spread by order of magnitude arguments and conclude that
beam spreading ceases after the perpendicular velocity attains
a certain (small) value. The final average number density
in the beam is shown by Gendrin[6] to correspond to a plasma
frequency about equal to the electron cyclotron frequency.

One of the key parameters determining the behavior
of collective effects is the ratio of the plasma frequency
to the electron cyclotron frequency. For altitudes above
the E-layer considered by Jones and Kellogg[8], this ratio
is generally greater than unity and approaches a maximum
value in the F-layer. In the E-layer itself the ratio is
much larger than unity. For altitudes beneath the E-layer,
however, the ratio decreases sharply as the plasma density
decreases. The low altitude region where $\omega_{pe}/\omega ce < 1$ was
of considerable interest in the low trajectory flight of
ZARNITSA-2. As we will show below, this is the same parameter
regime which describes the recent series of beam plasma
discharge (BPD) experiments carried out at Johnson Space
Flight Center.

In Table 5 we present data on ambient conditions
along a typical magnetic field line extending from the low
ionosphere up through the magnetosphere. This table will
be a useful reference in the determination of the importance
of collective effects for experiments of interest.

2.3.3   Absolute and Convective Instabilities

The behavior of the rocket fired electron beam
depends, of course, on the environment through which it
passes. In an Echo experiment, for example, where the beam
propagates through the magnetosphere, the beam may encounter
regions of turbulence established by naturally occurring
streams of particles. Such turbulent regions may scatter

as well as change the energy of the beam particles. The
effect of such processes depends on the origin of the turbulence.
It is for this reason that the study of beam interaction
with the magnetospheric plasma requires a knowledge of the
multitude of natural phenomena occurring in that region.

For the case that the environment can be considered
relatively stable, the beam can create its own level of
turbulence with which it can interact non-linearly. Unlike
the broad streams of plasma associated natural phenomena,
rocket fired beams have relatively small diameters, and
this feature of radial inhomogeneity can be important in
determining whether the beam plasma interaction will drive
parts of the wave spectrum unstable. The radial extent
of the beam usually can be taken to be of order of the electron
Larmor radius, and therefore a mode propagating in the beam
plasma system must have a radial wavenumber at least as
large as the inverse radius. In many cases this constraint
on the perpendicular wavenumber can have a stabilizing effect.
The finite radius also means that it is possible for an
unstable wavepacket to propagate across the system before
the instability has a chance to grow substantially. Thus,
when the instability is able to convect out of the region
of instability, the level of turbulence will remain very
low. On the other hand, the wavepacket will be able to
grow appreciably when:

$$\Gamma \equiv \frac{\rho_\perp \gamma}{V_{g\perp}} \gg 1$$

where $\rho_\perp$ is the beam radius, γ is the growth rate of the
mode, and $V_{g\perp}$ is the perpendicular group velocity. Γ is
a measure of the gain in the amplitude of the disturbance
as it propagates across the beam. In the limit of $V_{g\perp} \to 0$
a wavepacket does not convect away no matter how small the
region of instability or the growth rate is. Such an insta-
bility has been termed absolute (as opposed to convective
for non-zero V_g) by Briggs[9], who did pioneering work in

this field and pointed out a graphical prescription for
determining when V_g would vanish. Briggs' representative
construction occurs as a consequence of the inverse Fourier
transform used to obtain the spatial distribution of an
unstable wavepacket in the perpendicular (x) direction.
If a change of variables is made so that the integral over
K_x goes into an integral over ω, then the Jacobian factor
$\partial K_\omega(\omega)/\partial \omega$ is introduced into the integral. The factor is
formed through the requirement that the dielectric constant
$\varepsilon_o(K_x,K_z,\omega)$ remains zero as ω and K_x are varied:

$$\varepsilon_o(K_x,K_z,\omega) \simeq \frac{\partial \varepsilon_o}{\partial \omega}(\omega-\bar{\omega}) + \frac{\partial \varepsilon_o}{\partial K_x}(K_x - \bar{K}_x)$$

$$+ \text{ higher order terms} = 0$$

where $\bar{\omega}$ and $\vec{K} = \bar{K}_x \hat{X} + \bar{K}_z \hat{Z}$ are the frequency and wavenumber
of a growing mode ($\text{Im}\bar{\omega} > 0$ for a mode with $\exp(-i\bar{\omega}t)$ time
dependence), and $\hat{Z}$ is the unit vector in the magnetic field
direction. For this case we have the following single valued
relation for K_x as a function of ω:

$$K_x - \bar{K}_x = (\omega-\bar{\omega})/\mathcal{V}_{g\perp}$$

where:

$$\mathcal{V}_{g\perp} = \left(\frac{\partial \omega}{\partial K_x}\right)_{\bar{\omega},\bar{K}_x} = -\frac{\partial \varepsilon_o}{\partial K_x}\bigg/\left(\frac{\partial \varepsilon_o}{\partial \omega}\right)$$

and the group velocity $V_{g\perp} = R_e(\mathcal{V}_{g\perp})$. This type of relation
for a non-zero group velocity is characteristic of a convec-
tive mode. When $\mathcal{V}_{g\perp} \to 0$ so that $V_{g\perp}$ also $\to 0$, however, a dif-
ferent relation between K_x and ω results. For this case:

$$\varepsilon_o(K_x,K_z,\omega) = \frac{\partial \varepsilon_o}{\partial W}(\omega-\bar{\omega}) + \frac{1}{2}\frac{\partial^2 E_o}{\partial K_x^2}(K_x-\bar{K}_x)^2$$

$$+ \text{ higher order terms} = 0$$

so that now:

$$K_x - \bar{K}_x = \pm \left(\frac{- \dfrac{\partial \varepsilon_o}{\partial W}}{\dfrac{1}{2} \dfrac{\partial^2 \varepsilon_o}{\partial X^2}} \right)^{1/2} (\omega - \bar{\omega})^{1/2}$$

so that there now exist two branches of $K_x(\omega)$ in the vicinity of $\bar{\omega}$ and $\bar{K}_x$. The above behavior holds for ω and K_x very close to the unstable mode characterized by ω and K_x. The method of Briggs generalizes the above approach by examining the behavior of K_x over a prescribed region of ω. For the case that $\partial \omega / \partial K_x = 0$ within the interval of interest, a saddle-point will indicate the presence of the absolute instability.

The presence of convective rather than absolute instabilities in finite radius beam-plasma interaction allows for an effective stabilizing mechanism. Indeed, Jones and Kellogg[8] used the behavior of convective unstable whistler modes to argue that beams in the upper ionosphere/lower magnetosphere could retain their integrity while propagating. The analysis presented above also can be used to demonstrate the possible existence of steady state configurations where the growth is spatial rather than temporal. This situation exists when the dispersion relation is solved for $\vec{K}$ in terms of real ω rather than the other way around. It is clear that finite spatial growth is only meaningful for convective modes, where a unique relation for $\vec{K}$ in terms of ω exists. Note that the relation between the temporal growth rate γ and the spatial growth $\vec{K}_i$ is just $\gamma = \vec{V}_g \cdot \vec{K}_i$, so that the concept of spatial growth is not valid for absolute instability when $\vec{V}_g = 0$. The idea of steady state turbulent levels described by mode amplitudes obtained from spatial growth considerations in the inhomogeneous magnetosphere has led Ashour-Abdalla and Kennel[10]

to derive expressions for anomalous velocity diffusion coefficients. Such as analysis may be pertinent in (1) describing the fluctuation level of the magnetosphere environment through which a rocket fired beam propagates, or (2) suggesting how a steady state energetic particle distribution created by the rocket fired beam may become unstable.

2.3.4   RF Signals

The plasma and electron cyclotron frequencies are expected to be most characteristic of the rf signals obtained from the beam plasma interaction. The most complete published data on rf signatures of the beam plasma interaction in the ionosphere are due to Cartwright and Kellogg[11], who analyzed the ECHO I experiment. They show that signals at the ambient plasma frequency as well as strong bands of radiation at about twice the electronc cyclotron frequency were emitted. In addition, there are strong sources of radiation below the electron cyclotron frequency.

The measurements of the rf signals were made from a nose cone antenna, which was separated from the main rocket. The antenna was therefore immersed in the ionospheric plasma and obtained signals from the beam at ever increasing distances during the flight. The need for a nearby antenna for rf detection seems to be a necessary requirement for many rocket fired beam experiments. Ground based rf antennas were generally able to receive signals associated with only a limited number of the radiation sources detected by the nose cone antennas.

The observed plasma frequency radiation was computed by Cartwright and Kellogg as incoherent electrostatic Cerenkov radiation, and the value obtained was in agreement with the measurements. However, the amplitude of the signal unexpectedly peaked at about 5 ms into the 16 ms pulse

characteristic of ECHO I. In addition, the peak radiation occurred for those injected pitch angles just upfield from 90°. It was also expected that the radiation would drop off as the inverse of the square root of the distance between the nose cone antenna and the beam. The amplitude, however, did not vary according to this relation as the nose cone and beam separated from each other.

The observations of whistler modes ($f < f_{ce}$) also led to surprising results. Near apogee, a signal extending down only to a frequency of about $f_{ce}/2 \sim 500$ kHz was obtained, while at lower altitudes, whistlers were observed with frequencies down to 50 kHz, the frequency limit of the receiver. In addition, the radiation amplitude peaked within the beam pulse width just as with the plasma frequency waves. Again, the maximum amplitudes occurred for a pitch angle range just up field from 90°.

The radiation near $2 f_{ce}$ also has puzzling features. It is well known that for $f_{pe} > f_{ce}$, there is a cold plasma stop-band above f_{ce} that would preclude the existence of the lower harmonics of the electron cyclotron frequency. Thus, one would seem forced to explain the $2 f_{ce}$ in terms of warm plasma theory. Bernstein modes result from a warm plasma analysis and do have frequencies near the electron cyclotron harmonics. However, Cartwright and Kellogg point out that the Bernstein mode could explain the relatively large bandwidth of the $2 f_{ce}$ radiation only if the wavelength became very short and that such wavelengths could not be observed by the nose cone antennas. Further evidence of the second electron cyclotron harmonic has been reported by Monson and Kellogg[12] who carried out ground based rf antenna observations in conjunction with the ECHO IV experiment. Detection of these signals on the ground is significant because it implies an efficient conversion process through which a radio wave is produced.

The ARAKS experiments utilized a much larger beam current than in the case of ECHO I. Very much the same kinds of signals were observed by the nose cone antenna, except that the predominant electron cyclotron harmonies appeared to be n=4 rather than n=2. One important difference in the experiments was that the signals in ARAKS did not peak within the pulses but rather were continuous.

Strong ground based rf signals were detected from the ARAKS and ZARNITSA-2 experiments (Cambou et al[13]; Mishin an Ruzhin[14]) with frequencies in the tens of MHz range. This result is surprising since the largest frequency associated with the plasma is the upper hybrid which in the E and F layers takes on a value of about 3 MHz. In each of the experiments, the signal is attributed to the production of a high density plasma in the vicinity of the rocket. Creation of a plasma density about two orders of magnitude larger than the ambient density could explain the high frequency of the signals. An intensive analysis of the physics of plasma density enhancement has been carried out by Mishin and Ruzhin[14] with respect mainly to the ZARNITSA-2 experiment. According to Mishin and Ruzhin, the trajectory of the rocket was sufficiently low that the condition $\omega_{pe}/\omega_{ce} < 1$ was valid over nearly the entire flight. These authors propose for this case that the cyclotron resonance branch of the high frequency electron mode dispersion relation is ultimately responsible for the large plasma density enhancement. They argue that the fluctuating electric fields heat up the ambient electrons sufficiently to ionize the neutral particles present in the ionosphere. This mechanism, whereby plasma electrons are created by ionization of neutrals from ambient electrons heated by a beam plasma instability, is referred to as the beam-plasma discharge (BPD). The magnitude of the accelerating turbulence results from saturation of the linear modes. Mishin and Ruzhin have estimate a steady state-turbulence level by appealing

to the arguments of strong turbulence theory as well as
considering those levels appropriate to the weak turbulence
(quasi-linear) theory. In the former case, the theory of
weak turbulence breaks down because of a modulational insta-
bility. The mechanics of the stabilization of this parametric
mode to a final state including cavitons is not well understood
at this time, but the field is very active. It has yet
to be determined, conclusively, whether strong turbulence
is responsible for naturally occurring rf phenomena. Of
particule importance in the theory is that a critical neutral
number density exists, above which more particles are created
through ionization processes than are lost by diffusion.
The value for this number allows for an experimental check
to the theory.

Having discussed the conditions for BPD, Mishin
and Ruzhin finally determine the conversion efficiency of
the electrostatic mode (basically Langmuir oscillations)
to a radio wave that can be received at a ground based antenna.
Two processes have been considered. One is wave fusion
of the longitudinal wave with an ion sound mode ($\ell + s \rightarrow t$).
The other suggested process is the fusion of the Langmuir
wave with still another longitudinal wave, the Bernstein
mode ($\ell + \ell \rightarrow t$).

The HF results from the ZARNITSA-2 experiment
as well as the theory for $\omega_{pe} < \omega_{ce}$ are of particular inter-
est to American investigators since BPD ground experiments
in which an electron gun is fired into a gas filled chamber
have been carried out by Bernstein et al.[15] An ambient
magnetic field was established within the chamber and the
pitch angle of the injected beam was about 20°. The chamber
pressure of $10^{-5} - 10^{-6}$ T as well as the magnetic field
strength of just over 1 G are indicative of conditions in
the lower ionosphere. The beam energy of $\sim$ 1 keV was much
lower than that characteristic of rocket fired beam experiments.
Since the background gas was not pre-ionized, an ambient

backgroun plasma had to be created by direct ionization from the beam. Thus, for low beam currents (prior to BPD), the condition $\omega_{pe} < \omega_{ce}$ was satisfied. The experiments showed that at a critical current, the electron number density increased dramatically. It is not yet clear that the BPD chamber experiments have been adequately explained. Bernstein et al.[15] have compared the experimental results with a theory by Lyachov and Manadadze[16], who have done work on the ZARNITSA-2 experiment, and have concluded that the predicted critical neutral density was an order of magnitude higher than required in the experiment. Rowland and Papadopoulos[17] have postulated that BPD for $\omega_{pe} < \omega_{ce}$ is triggered by the onset of the Cerenkov beam mode coupled with the slow cold electron plasma mode. A critical ambient plasma density is required for onset of the mode. Rowland and Papadopoulos claim that their model explains the experimental scaling.

BPD appears to occur when beams are fired within the E and F layers where $\omega_{pe} > \omega_{ce}$. This case has been treated in less detail then for $\omega_{pe} < \omega_{ce}$, and no ground based chamber experiments have as yet been carried out in this regime.

2.3.5   Turbulence and Anomalous Beam Transport

Rocket fired electron beam experiments have given ample evidence of the presence of important collective effects. Some of the observed phenomena which cannot be explained on the basis of particle-particle interaction are: enhanced local backscatter in upward injection; diffuse streak effects in downward injection; excessive particle flux losses in echoing experiments; and, long delay times in the return of particles that have mirrored.

effect will eventually heat the plasma so that the mode
would continue to grow when kinetic considerations are taken
into account. It has long been felt that a final saturation
level could be formed by the method of weak turbulence,
but this no longer may be the case. It has been determined,
for example, that Langmuir turbulence cannot be described
by weak turbulence theory whenever $W/nT > (K\lambda_D)^2$, where
W is the turbulent energy density, T is the plasma temperature,
and λ_D is the Debye length.[23] The subsequent behavior
of this strong or spiky turbulence has not been well
established.

In mirroring (or echo) experiments where the beam
propagates within the magnetosphere, it is important to
consider the turbulent spectrum caused by natural effects.
In this regard, an interesting analysis has been carried
out by Ashour-Abdalla and Kennel[10]. These authors assumed
the presence of a stationary spectrum based on spatial growth
profiles existing in the inhomogeneous magnetosphere. The
basic linear instability considered was the upper hybrid
electrostatic electron mode being driven by electron cyclotron
resonances associated with a hot component with loss cone
anisotropy. The analysis finally allows for determination
of a turbulent spectrum which would be part of the ambient
background through which a rocket fired electron beam would
propagate. There is a large literature on magnetospheric
structure, and this is an area of importance in beam propa-
gation studies. A recent representative work in this field
is a paper by Kan and Akasofu[18], who discuss the structure
of the magnetosphere-ionosphere required to support an auroral
electric field. The role of the whistler mode in magneto-
spheric turbulence was first emphasized in an important
paper by Kennel and Petschek[19], and their notion of a
flux limit on stably trapped particles in the magnetosphere
has recently attracted much attention.[20, 21]

As discussed above, determination of the turbulent
spectrum for beam plasma interaction must proceed mainly
on theoretical grounds. There is a rather good justification
for examining the high frequency electrostatic electron
mode driven by beam Cerenkov or cyclotron interaction as
being response for self-generated turbulence. Analysis
of this mode for cold beam has been examined in some detail
by Papadopoulous[22] for finite systems in the respective
limits of large magnetic field and large plasma density,
respectively. On the other hand, the mechanisms responsible
for saturation of the linear mode are not well understood.
The beam may become trapped within its own field, but this

effect will eventually heat the plasma so that the mode
would continue to grow when kinetic considerations are taken
into account. It has long been felt that a final saturation
level could be formed by the method of weak turbulence,
but this no longer may be the case. It has been determined,
for example, that Langmuir turbulence cannot be described
by weak turbulence theory whenever $W/nT > (K\lambda_D)^2$, where
W is the turbulent energy density, T is the plasma temperature,
and λ_D is the Debye length.[23] The subsequent behavior
of this strong or spiky turbulence has not been well
established.

RESULTS AND THEIR INTERPRETATION WITH RESPECT TO ECHO-4 DATA

3.1   TEST RUNS OF MCBE

We have carried out important test runs of MCBE, a Monte-Carlo algorithm for the transport of multi-keV electrons along magnetic field lines. The code has been used to simulate downward rocket-fired electron beam scattering and deposition in the ionosphere. Using Gouldsmit-Saunderson multiple scattering theory, we have determined the beam width in the region of energy deposition. Identification of these results with beam width measurements of artificial aurora shows that the model accurately computes the beam width resulting from particle-particle effects. We believe that MCBE gives the best available predictive capability for classical beam widths as functions of the requisite beam parameters--energy and pitch angle.

Several test runs were carried out. Figure 2 shows the energy deposition of 20 keV electrons injected downward into the ionosphere from 300 km at 0° pitch angle as a function of altitude. The dotted curve represents deposition results from Berger et al.[24] In both cases, maximum deposition occurs at about 100 km and the results are in good quantitative agreement. A similar plot is shown in Figure 3 where deposition is into a N_2 atmosphere, and the energy distribution is 10 keV gaussian. The broken curve gives results from B3C, an algorithm
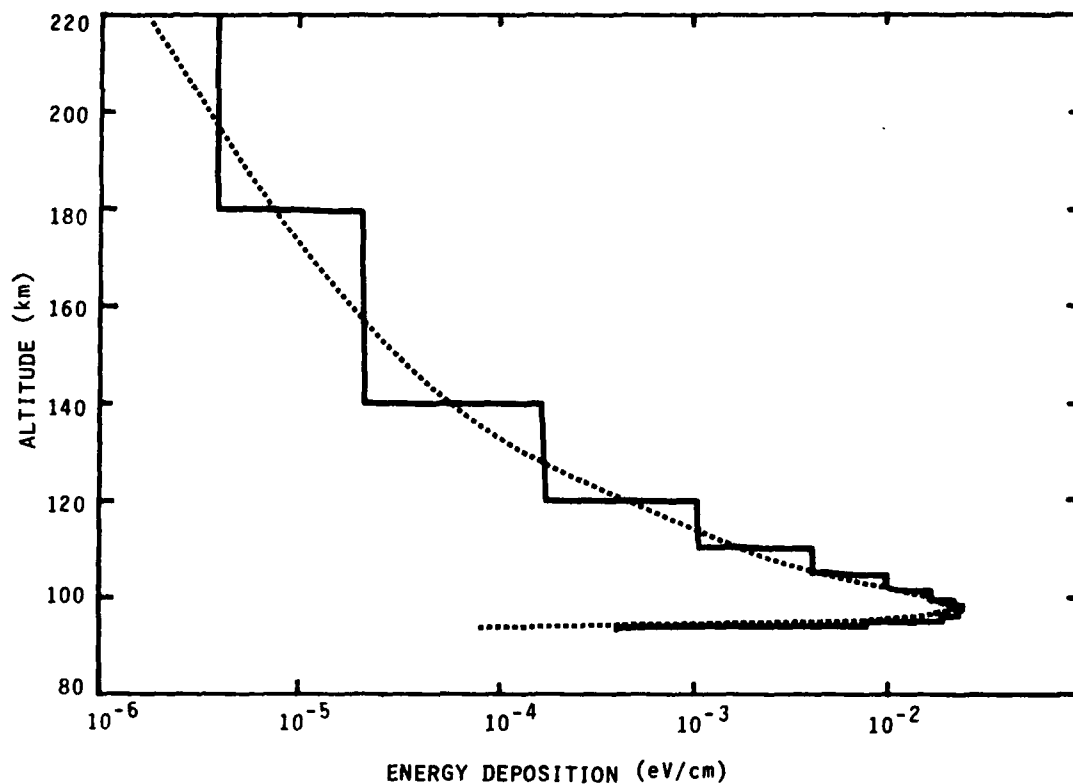
FIGURE 2. Energy Deposition as a Function of
Altitude for Downward Injection of 20 keV Electrons
from 300 km at Normal Incidence

The solid histogram is the MCBE result, while
the dotted curve gives the result of Berger,
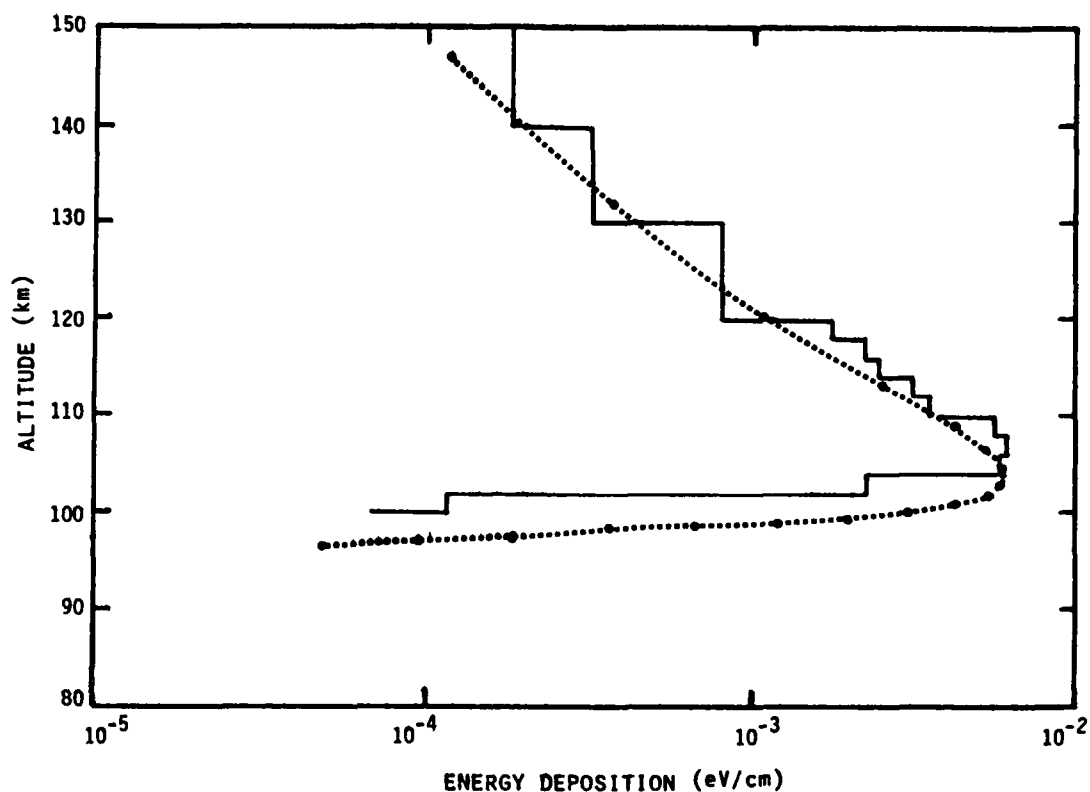et al.[24]

FIGURE 3. Energy Deposition as a Function of
Altitude for Downward Injection at Normal Incidence

Energy Distribution is 10 keV Gaussian. The solid
histogram is the MCBE result, while the broken curve
is the result from the B3C algorithm.

developed by SAI to give optical emissions from electron deposition. In this case, MCBE was run with 1000 histories and computed 26% backscatter across the injection plane. The corresponding percentage for B3C was 24%. The effect of initial pitch angle on the deposition profile is shown in Figure 4 for 20 keV electrons. The light solid curve represents an isotropic distribution of downward directed pitch angles. Results for 45° pitch angle injection are given by the dotted curve, while the deposition of normally incident electrons are shown by the heavy solid curve. Deposition profiles for normal incidence for a family of electron energies are presented in Figure 5. Results for energies of 10, 20, and 30 keV are plotted.

Figure 6 presents the effective beam width as a function of altitude for 20 keV electrons injected normally (solid curve) and isotropically (dotted curve). The interesting point here is that electron scattering substantially spreads out normally incident electrons so that at the lower altitudes where deposition and optical emissions occur, the beam spread is effectively independent of initial pitch angle distribution. Note that the effective beam radius is less than the characteristic quantity $2|\chi|/\omega_{ce}$ that gives a measure of the maximum gyro-radius. This result will be discussed further in the next section.

3.2 INTERPRETATION OF ARTIFICIAL AURORA EXPERIMENT IN ECHO-4 ROCKET LAUNCH

3.2.1 Comparison with MCBE Results

The generation of artificial aurora in ECHO 4 rocket launch (Hallinan et al.[25]) serves as a relevant test for the analyses developed in the AFGL program. A
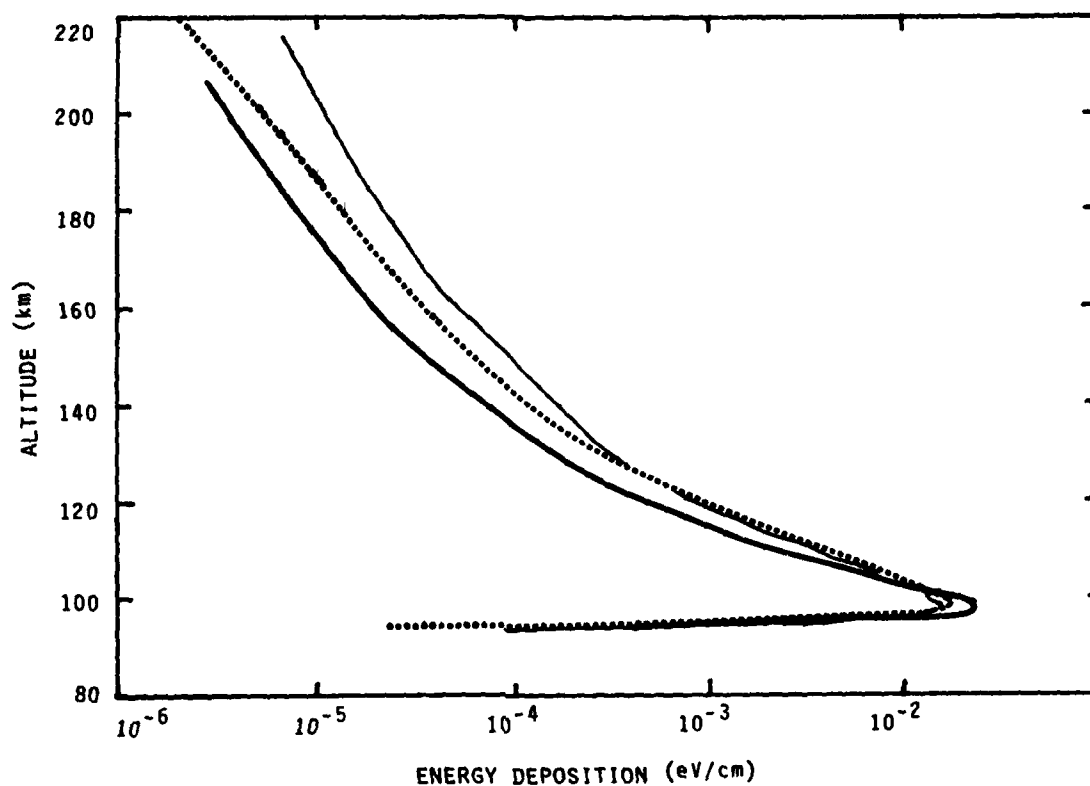
FIGURE 4. Energy Deposition as a Function of
Altitude for Downward Injection of 20 keV Electrons
from 300 km

The light solid curve represents an isotropic
distribution of downward directed pitch angles.
The dotted curve represents 45°, while the heavy
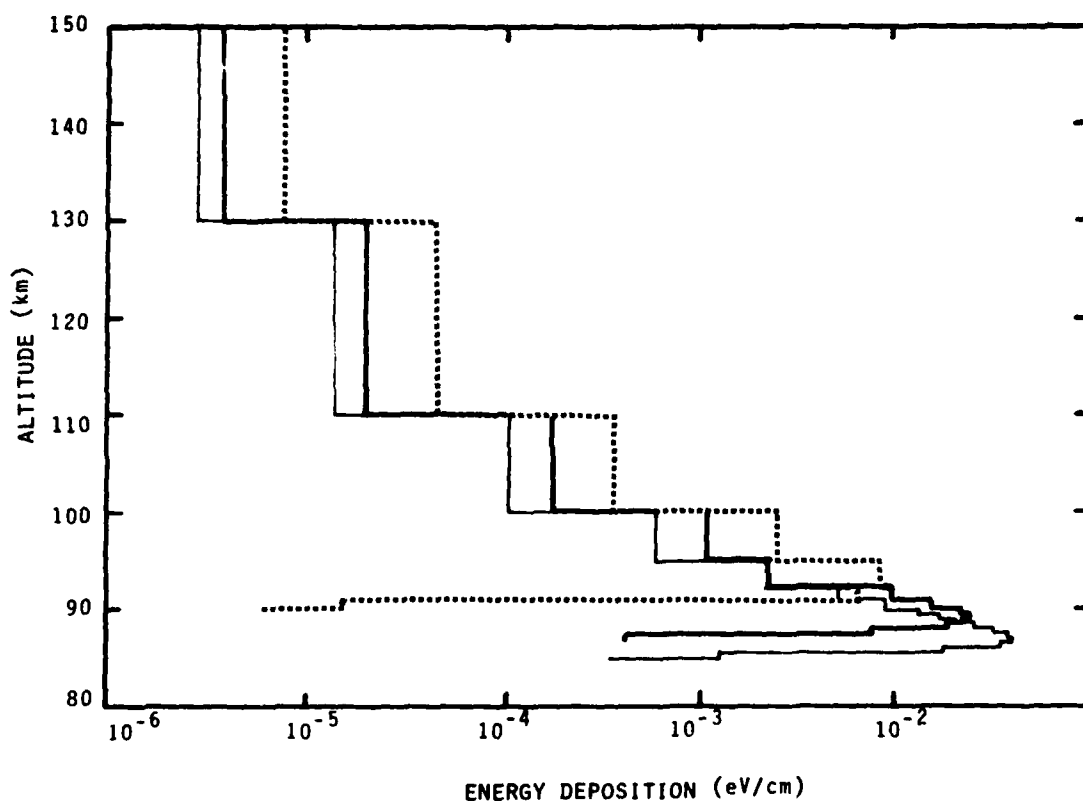solid curve shows the results for normally incident
electrons.

FIGURE 5. Energy Deposition as a Function of
Altitude for Downward Injection from
300 km of Electrons of Various Energies

The dotted histogram shows results for 10 keV electrons;
the heavy solid histogram indicates results at 20 keV;
the light solid histogram shows results for 30 keV
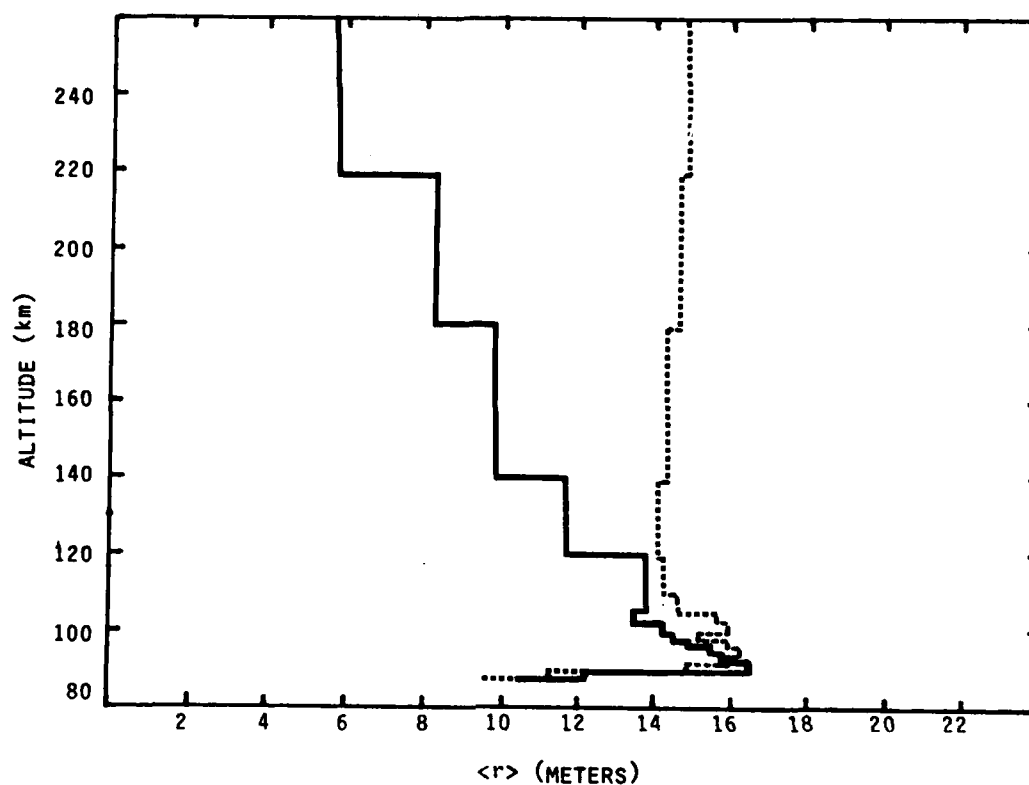electrons. In all cases, the pitch angle is 0°.

FIGURE 6. Effective Beam Width as a Function of
Altitude for Downward Injection from
300 km of 20 keV Electrons

The solid histogram shows results for normal incidence,
while the dotted histogram gives results for an
isotropic pitch angle distribution.

capsule description of the ECHO series of experiments is
given in the previously presented Tables 1-5 and in Figure 1.
The experiment was particularly interesting because the radial
extent of the beam could be resolved. A summary of the
streak width results is given in Table 6.

Optical emissions from the artificial aurora
emanated from the region of maximum energy deposition,
between 100 and 90 km. As shown in Table 6, the observed
streak widths depended strongly on the altitude at which
the gun was fired. At rocket apogee, streak diameters well
in excess of 100 m were found, and these were called diffuse
aurora. All other examples were referred to as normal
streaks, although it is seen that there is a considerable
variation in the streak widths at the other firing altitudes.
Hallinan et al.[25] interpreted the diffuse aurora as being
the result of wave-particle effects, but they generally
attributed the other test results to classical effects. We
believe that their interpretation followed from the results
of Berger et al.[24] who presented beam widths in excess of
100 m due solely to particle-particle effects. The corre-
sponding results from MCBE, as shown in Figure 6, give
much smaller streak widths due to particle-particle inter-
actions. The width of the beam at auroral altitudes is
between 32 and 33 m, in good agreement with the ECHO 4 streak
width observed for a firing altitude of 148 km. Although
the energies, as well as the pitch angle ranges, for this
firing are not the same as in the MCBE run, the signifi-
cance of the numerical results is clear. The streak
widths due to particle-particle interactions are
relatively small, and significant increases in the widths
must be due to other effects, such as wave-particle

TABLE 6.   SUMMARY OF ECHO 4 STREAK WIDTH OBSERVATIONS

FIRING ALTITUDE (km)	ENERGY (keV)	$\hat{r}_e$ (m)	STREAK WIDTH (m)	PITCH ANGLE (°)
148 (UPLEG)	26	11.8	34	70
160	36	13.9	44	70
210	26	11.8	182	70
214	38	14.3	128	30-90
181 (DOWNLEG)	34	13.5	72	70
156	33	13.3	59	30-90

$$\hat{r}_e \equiv \frac{1}{\omega_{ce}} \sqrt{\frac{2E}{m}}$$

interaction. We therefore conclude that wave-particle
interaction plays a role in firings between 148 km and
apogee. The effects are continuous, becoming stronger
as the altitude increases.

3.2.2   Wave-Particle Effects in Artificial Aurora

Any study of wave-particle effects involves the
accurate specification of equilibrium conditions. In
rocket fired e-beam experiments, we have found that one of
the major problems is beam characterization. In most
experiments, the electrons are injected at a particular
pitch angle. For such cases, the single particle tra-
jectories fall on a helix wound about a cylinder along
the magnetic field line with Larmor radius $V_\perp/\omega_{ce}$, where
$V_\perp$ is the electron velocity component perpendicular to the
magnetic field and ω_{ce} is the electron cyclotron frequency
(eB/mc in cgs units). A pulse of electrons would occupy
a finite length sector of the helix. Since the pulse width
is much larger than the time for an electron to complete a
cyclotron orbit, the axial length of a single pulse is of
order thousands of time longer than the Larmor radius.
Space charge effects can change this picture however. If
the number density of the beam at the gun orifice is larger
than the ambient plasma density, the beam will expand at
least until the beam density reduces to the ambient density,
at which point the charge begins to be neutralized. This
will give rise to velocity dispersion. For example,
following Gendrin,[7] we can estimate:

$$\frac{\Delta V_\|}{V_\|} \sim \left(\frac{I}{I_c}\right)^{\frac{1}{2}}$$

3-10

where I_c is space charge limited current. For experiments of interest where E = 25 keV, I_c = 131A. For ECHO 4 currents 70 mA, this yields a 2% velocity dispersion, which for pitch angles of 60° is sufficient to "fill in" the space between the initial helical windings in about 1 mile. Of course, even this scenario can be made more complex by efforts occuring closer to the rocket, namely instabilities associated with the helical tube which may be associated with beam plasma discharge (BPD). At any rate, it seems reasonable to assume that the beam can be characterized by reasonably symmetric shells within a few kilometers of the injection point. If this configuration gives rise to an instability, then the electric field that develops opposes the electron motion (i.e., reducing the beam kinetic energy). This means that $\underset{\sim}{E} \times \underset{\sim}{B}$ is directed outward so that the electrons will drift outward, thus increasing the radius of the beam.

It has been well established that the hollow beam configuration to which the helix has evolved is unstable to two stream modes. In the simplest two stream analysis, the streaming velocity is parallel to the magnetic field. The hollow beam development, however, is due to the transverse anisotropy of the electron pulses. This configuration can be shown to produce instability analogous to the usual two stream result. The nonlinear saturation of the cold electrostatic wave is due to particle trapping. The field amplitude at saturation scales as

$$\frac{E^2}{8\pi} = \alpha N_b \varepsilon_b$$

where ε_b is the beam particle energy and α is a dimension-less factor between about 0.1-0.3. The magnitude of the

$\underset{\sim}{E}$ x $\underset{\sim}{B}$ drift of resonant particles is therefore

$$V_D = \frac{cE}{m} = \alpha^{\frac{1}{2}} \frac{\omega_b}{\omega_{ce}} V_b$$

where V_b is the beam particle speed.

We now compute the time required for the beam to
spread out to a radius of 91 m, the largest streak width
observed in the ECHO 4 experiments. Typical beam para-
meters for the experiments are electron energies of 25 keV
and pitch angles of 60°. For simplicity, we assume that
the beam is solid rather than hollow and has an initial
radius equal to the Larmor radius. Since the Larmor radius
is only 10m, consideration of a solid cylinder cannot
change the result significantly. The beam plasma frequency
varies inversely with the expanding radius, so

$$\omega_b = \frac{\omega_{b0}}{r} r_L$$

where ω_{b0} is the initial beam plasma frequency correspond-
ing to the cylinder of radius r_L. The equation for the
expanding radius is just

$$\frac{dr}{dt} = \alpha^{\frac{1}{2}} \frac{\omega_{b0}}{r} \frac{r_L V_b}{\omega_{ce}}$$

Letting $\alpha = 0.1$ and $B = 0.46G$, we find that the beam width
evolves to 91 m radius in a distance of 17 km from the gun
injection point.

In order for the drift to be sustained, the
system must remain collisionless. This means that the
higher energy electrons may not undergo collisions with

neutrals during the wave growth period. The growth rate for many modes of interest is of order

$$\gamma \sim \omega_p \left(\frac{n_b}{n_b}\right)^{\frac{1}{3}} = 1.6 \cdot 10^6 \ \text{sec}^{-1}$$

For a nighttime density, $n_D = 2 \cdot 10^3$ at altitudes between 100 and 200 km, the growth rate for a 200m diameter beam with the aforementioned parameters is

$$\gamma = 1.33 \cdot 10^5 \ \text{sec}^{-1}$$

These growth rates are much higher than the primary electron collision frequencies. In fact, 25 keV electrons experience a collision frequency with neutrals of only about $1.8 \cdot 10^5 \text{sec}^{-1}$ at an altitude as low as 130 km. Hence, for altitudes above this, the beam plasma system is effectively collisionless. The question arises as to why even greater beam expansions than indicated by the maximum observed diameters of ~ 200m do not occur. The reason may be that the type of mode changes. Note that the plasma density for which $\omega_p = \omega_{ce}$ is just

$$n_p = 2.06 \cdot 10^4 \text{cm}^{-3}$$

For nighttime electron densities associated with artificial aurora experiments, the plasma density may be smaller than this value at altitudes of 200 km and below. In this region, the excited modes would be subject to the condition $\omega_{ce}/\omega_p >> 1$. This change in the mode topology may be effective in terminating the large amplitude fluctuation spectrum. On the other hand, these modes may still be responsible for streak widths greater than those expected from particle-particle interactions occurring at the firing altitudes under 200 km.

The above analysis suggests that diffuse aurora (where beam widths are much greater than 100m) will occur whenever the plasma frequency is larger than the electron cyclotron frequency. Our interpretation of why beam spread may decrease considerably for beam propagation under 200 km as well as the computed spread ratio in regions where $\omega_p/\omega_{ce} > 1$ are consistent with experiment where diffuse aurora were obtained for beam injection altitudes of 210 km and 214 km. It is interesting to note that beam spread is insensitive to the beam number density (i.e., the beam current for given energy and pitch angle). For a given distance along the field line over which the instability develops, the beam spread varies only as $n_b^{\frac{1}{4}}$. Such insensitivity of the width of an artificial aurora to beam current can easily be checked by experiment.

Other factors need be considered before the above theory can indeed be verified. First, the evolution of the helical beam to a neutral hollow cylinder and then, perhaps a solid cylinder needs to be investigated experimentally, relatively close to the electron gun. Second, the temperature of the beam should be determined. If the beam heats up rapidly, the instability will shift from the hydrodynamic "cold" mode to a kinetic "hot" mode. Such modes not only have smaller growth rates in the linear regime, but may be susceptible to caviton formation in the nonlinear regime. It has been suggested that cavitons could accelerate ambient electrons to high energies. It would be of interest to measure the particle spectrum to determine whether this effect occurs. A third factor is that the changes in mode structure can influence the convective nature of the instability, so that whereas a cold plasma mode may remain effectively stationary in radial

position, a warm mode may convect quickly out of the
generation region before the fluctuation level becomes
large enough to influence particle orbits. The problem
of mode convection within warm finite beams is yet to be
addressed.

Section 4

SUGGESTIONS FOR ROCKET FIRED BEAM EXPERIMENTS
AT AFGL

4.1   ION BEAM PROPAGATION

One of the interesting results from the spacecraft charging experiment of Cohen was the fact that the return current very closely equalled the emitted 8 µA ion current, irrespective of the rocket altitude. At the high altitudes, where the ambient ion density is high, this finding is not surprising since the return current can be obtained from the large reservoir of electrons traveling no faster than the thermal speed. At an altitude of 150 km, however, where the ambient density is only 10^3, this argument would yield a return current of less than 0.1 µA. Thus, the soruce of the measured return current at low altitudes is not readily apparent. It has been often suggested that the fluctuating electric fields arising from plasma instability may increase the number density by accelerating the secondary electrons to energies above the threshold for ionization of the background neutral particles. The accompanying enhancement of the background electron number density could be sufficient to produce the required return current. We propose that the r.f. signatures of instabilities caused by ion beams should be monitored.

The use of ion beams in rocket fired beam experiments should allow for the excitation of VLF electrostatic modes. According to theory, the hydrodynamic magnetized ion-ion instability should be present for the low velocity xenon ion guns that have been used by Cohen on a sounding

4-1

rocket and on the SCATHA satellite. The mode propagates
almost perpendicular to the magnetic field, while it is driven
by a beam directed at least partly across the magnetic field
line.

The major condition for driving the mode is that
the beam particle speed be less than a quantity of order
the Alfven speed:

$$V_A = \frac{B}{\sqrt{4\pi n M_i}}$$

For ionospheric altitudes where O^+ is the dominant ion species,
$V_A = 4 \cdot 10^7$ cm/sec. It is relatively easy to create an ion
beam with small enough particle velocities. Since the xenon
atom is so massive, the velocity of 1 keV beam particles
is only $3.8 \cdot 10^6$ cm/sec, well below the Alfven speed threshold.
In fact, the greater challenge is to install on a rocket
an ion gun where beam particle speeds can be made to exceed
the Alfven speed, so that the ion-ion instability can be
avoided.

The mode frequency will be near the lower hybrid
frequency, which, for ionospheric parameters of interest,
is about equal to the ambient ion plasma frequency. In the
region where O^+ is dominant, and where we take an average
density of 10^5 cm^{-3}, we find an expected mode frequency
$\omega \simeq 10^5$ rad/sec or f = 17 kHz, i.e., within the VLF range.
The instability growth rate is also of order of the lower
hybrid frequency and is much larger than typical ion collision
frequencies. Thus, collisional damping effects can be ignored.

The above mode is magnetic in the sense that the wave number must be much smaller than the inverse electron Larmor radius. On the other hand, the mode is stabilized when the wave number is so small that an electromagnetic term in the dispersion relations takes on a large value. The first condition implies that the wavelength cannot be smaller than about 10 cm (where an ambient temperature of 0.1 eV has been assumed). The second condition can be shown to limit the wavelength to tens of meters. For the xenon beam conditions quoted above, the maximum growth rate for the linear instability will occur for a wavelength of about 1 m.

The instability can be expected to most affect the beam properties when the beam density is comparable to the ambient density. If the beam density at the nozzle is larger than the ambient density, then it is generally accepted that the beam will spread out until a stationary configuration is achieved. The density is expected to decrease to near the ambient level at which point the beam would be charge neutralized. Therefore, the resulting beam plasma coupling would be strong. The level of ion current needed to trigger the instability would be that value for which the beam density just equalled the ambient density at the gun nozzle. The current corresponding to a beam density of 10^5 cm^{-3} entering a 5 cm diameter nozzle is just over a μA. Increase of the current enhances the volume over which the interaction would take place and, therefore, produces a stronger signal. It has been suggested, however, that a beam that is initially non-neutral may attain a steady unneutralized configuration. For the case of electron beam experiments, it is still not clear whether the beams are actually neutral. The absence of charge neutrality in an ion beam experiment could prevent the strong beam plasma coupling we have been discussing.

4.2 DETECTION OF ELECTROMAGNETIC SIGNALS ON NOSE CONE ANTENNA

The use of nose cone antennas has been an important feature of the ECHO experiments in the reception of r.f. signals. The nose cones are ejected from the rocket and have been used to monitor signals at distances of a few meters to about 1 kilometer from the beam. Since it is generally supposed that electrostatic signals are most strongly excited in the beam plasma interaction, the r.f. antennas in the ECHO series have been capable of measuring only electric fields. It is of interest, however, to monitor the presence of electromagnetic waves with the nose cone antenna. It should be possible to measure the fluctuating magnetic field with two small lightweight loop antennas oriented at right angles to each other. Not only will this diagnostic allow for the pickup of direct electromagnetic signals from the region of beam plasma interaction, but, perhaps more importantly, it will allow for the detection of electrostatic modes that are converted to electromagnetic signals. The conversion mechanism of the plasma mode to a vacuum signal is well known. In addition, however, the ECHO experiments have picked up signals at twice the electron gyrofrequency on the ground, as well as on electrostatic nose cone antennas. This mode has generally been identified as the Bernstein mode which propagates nearly perpendicular to the ambient magnetic field. At present, the conversion mechanism is not known. The ability to detect an electromagnetic signal at twice the gyrofrequency (≈ 3 MHz) would permit the determination of whether or not conversion occurs in the vicinity of the rocket. Even a negative result here would be of interest, because it would prove that the conversion took place away from the rocket at some well-defined position in the ionosphere. There are, for example, theories suggesting that conversion takes place because of ambient density gradients.

We believe that Langmuir probes should be attached
to the nose cone to monitor the fluctuation level of those
modes that propagate away from the interaction region. Since
the characteristics of modes propagating within a stable
plasma away from the source region are fairly well-understood
in terms of group velocities and damping rates, it should
be possible to reconstruct the fluctuation data to evaluate
conditions within the interaction zone. Ed Szuzczesicz wants
to attempt fluctuating measurements on the shuttle. He informs
us that the power supply required for the modulated signal
on the probes weigh only five pounds. It thus may be possible
to incorporate such a diagnostic on a rocket nose cone.

4.3   CURRENT NEUTRALIZATION AND ROCKET CHARGING EXPERIMENTS

As discussed before, one of the important aspects
of beam ejection from rockets is the avoidance of potential
build-up. It is easy to show that in the absence of return
current, even moderate current outflow will rapidly increase
the vehicle potential so as to shut down the current. Under
many conditions, the return current thought to be available
from the ambient plasma is not suffici t to produce the
required neutralization. Interestingly, however, neutralization
seems to occur under most conditions of beam injection. The
myriad processes that must cause neutralization are not under-
stood, and we suggest a program to examine this question.
The key aspect of this experimental effort would be to modulate
the magnitude of the beam current. As the current increases,
it is expected that the following sequences of neutralization
processes will occur:

- flow of thermal ambient electrons
  toward vehicle;

- potential enhanced flow of ambient electrons;

- ionization of neutrals to enhance electron
  number reservoir about vehicle (Beam Plasma
  Discharge).

With currents available of order 1A, it is expected
that the threshold of the beam plasma discharge (BPD) will
be achieved. Here it is of particular interest to test the
ionospheric scaling and compare this with the scaling achieved
at the Johnson Space Center. The results of the laboratory
experiments suggest the BPD is not very sensitive to pitch
angle, and this is another result that this experiment could
verify.

Section 5

REFERENCES

1. Hess, W. N., M. C. Trichel, T. N. Davis, W. C. Beggs, G. E. Kraft, E. Stassinopoulos, and E. J. R. Maier, "Artificial Auroral Experiment: Experiment and Principal Results", J. Geophys. Res., 76, 6067-6081, 1971.

2. Davis, T. N., T. J. Hallinan, G. D. Mead, J. M. Mead, M. C. Trichel, and W. N. Hess, "Artificial Auroral Experiment: Ground-Based Optical Observations", J. Geophys. Res., 76, 6082-6092, 1971.

3. Davis, T. N., "Television Observations of Artificial Aurora and Analyses of Flight Data from NASA Payload", 12.18 NE, Final Report, NASA Contract Number NAS9-11815, Geophys. Inst., Fairbanks, Alaska, October 1974.

4. Winckler, J. R., "The Application of Artificial Electron Beams to Magnetospheric Research", Cosmic Physics Technical Report 183, University of Minnesota, Minneapolis, Minnesota, October 1979.

5. Cohen, H. A., C. Sherman, and E. G. Mullen, "Spacecraft Charging Due to Positive Ion Emission: An Experimental Study", Geophys. Res. Lett. 6, 515-518, 1979.

6. Alekhin, Ju. K., V. I. Karpman, D. D. Rjutov, and R. Z. Sagdeev, "On the Stability of an Electron Beam Injected Along the Geomagnetic Field", Cos. Electrodyn. 2, 280-291, 1971.

7. Gendrin, R., "Initial Expansion Phase of an Artificially Injected Electron Beam", Planet. Space Sci., 22, 633-636, 1974.

8. Jones, J. W. and P. J. Kellogg, "Plasma Waves Artificially Induced in the Ionosphere", J., Geophys. Res., 78, 2166-2175, 1973.

9. Briggs, R. J., Electron-Stream Interactions with Plasmas, MIT Press, Cambridge, Massachusetts, 1964.

REFERENCES (*Continued*)

10. Ashour-Abdalla, M. and C. F. Kennel, "Nonconvective and Convective Electron Cyclotron Harmonic Instabilities", J. Geophys. Res., 83, 1531-1543, 1978.

11. Cartwright, D. G. and P. J. Kellogg, "Observations of Rdiation from an Electron Beam Artificially Injected into the Ionosphere", J. Geophys. Res., 79, 1439-1457, 1974.

12. Monson, S. J. and P. J. Kellogg, "Ground Observations of Waves at 2.96 MHz Generated by an 8- to 40-keV Electron Beam in the Ionosphere", J. Geophys. Res., 83, 121-131, 1978.

13. Cambou, F., J. Lavergnat, V. V. Migulin, A. I. Morozov, B. E. Paton, R. Pellat, A. Kh. Pyatsi, H. Rème, R. Z. Sagdeev, W. R. Sheldon, and I. A. Zhulin, "ARAKS — Controlled or Puzzling Experiment?", Nature, 271, 723-726, 1978.

14. Mishin, E. V. and Yu. Ya. Ruzhin, "Beam-Plasma Discharge During Electron Beam Injection in Ionosphere; Dynamics of the Region in Rocket Environment in ARAKS and ZARNITSA-2 Experiments", Preprint Number 219, Institute of Terrestrial Magnetism, Ionosphere, and Radiowave Propagation, Moscow, 1978.

15. Bernstein, W., H. Leinbach, P. Kellogg, S. Monson, T. Hallinan, O. K. Garriott, A. Konradi, J. McCoy, P. Daly, B. Baker, and H. R. Anderson, "Electron Beam Injection Experiments: The Beam-Plasma Discharge at Low Pressures and Magnetic Field Strengths", Geophys. Res. Lett., 5, 127-130, 1978.

16. Lyachov, S. B. and G. G. Managadze, "Beam-Plasma Discharge Near the Rocket (ZARNITSA-II-Experiment)", Space Research Institute Academy of Sciences of the USSR, Report Number 310, Moscow, 1977.

17. Rowland, H. L. and K. Papadopoulos, Private Communication, 1979.

18. Kan, J. R. and S. -I. Akasofu, "A Model of the Auroral Electric Field", J. Geophys. Res., 84, 507-512, 1979.

19. Kennel, C. F. and H. E. Petschek, "Limit on Stably Trapped Particle Fluxes", J. Geophys. Res., 71, 1-28, 1966.

REFERENCES (*Concluded*)

20. Baker, D. N., P. Stauning, E. W. Hones, Jr., P. R. Higbie, and R. D. Belian, "Strong Electron Pitch Angle Diffusion Observed at Geostationary Orbit", Geophys. Res. Lett., 6, 205-208, 1979.

21. Trefall, H. and D. J. Williams, "Time-Structure of Post-Midnight Energetic Electron Precipitation and the Limit of Stable Trappling", J. Geophys. Res., 84, 2725-2735, 1979.

22. Papadopoulos, K., Private Communication, 1979.

23. Sagdeev, R. Z., "The 1976 Oppenheimer Lectures: Critical Problems in Plasma Astrophysics, I. Turbulence and Nonlinear Waves", Rev. Mod. Phys., 51, 1-9, 1979.

24. Berger, M. J., S. M. Seltzer, and D. Maeda, J. Atmos. Terr. Phys., 32, 1015 (1970).

25. Hallinan, T. J., H. C. Stenback-Neilson, and J. R. Winckler, "The Echo 4 Electron Beam Experiment: Television Observation of Artificial Auroral Streaks Indicating Strong Beam Interactions in the High-Latitude Magnetosphere", J. Geophys. Res., 83, 3263, 1978.

APPENDIX

Determination of Artificial Auroral Streak Widths Using Guiding Center Diffusion Theory

D. L. LIN[1]

Radiation and Electromagnetics Division, Science Applications, Inc., Vienna, Virginia 22180

D. J. STRICKLAND

Beers Associates, Inc., Reston, Virginia 22090

The theory of two-dimensional random walk is applied to the problem of guiding center diffusion of kilovolt electrons caused by particle-particle interactions. The mean radius of the guiding center distribution is shown to depend, in a simple way, on the scattering and energy loss properties of the interactions. A formula for the width of an artificial auroral streak is derived which is consistent with observations and Monte Carlo results.

INTRODUCTION

This paper addresses the problem of the spreading of an electron beam under the influence of particle-particle interactions in the presence of a magnetic field. The specific application is to rocket-fired electron (e) beams in the ionosphere. The basic quantity to be derived is the average radius of energy deposition. The work is analytic and considers such key parameters as the Goudsmit-Saunderson multiple scattering distribution, a single scattering distribution, and the probability distribution for random walking in two dimensions. The analytic model was developed to provide physical insight into results being generated by a recently developed Monte Carlo code which describes the transport of kilovolt beam electrons in the converging geomagnetic field at ionospheric altitudes. A paper is now being written describing the capabilities of this code and results, which are directly comparable with experiment.

In addition to the desire for physical insight, the work being reported was also motivated by discrepancies between predicted beam spreading using the above Monte Carlo code and that of *Berger et al.* [1970]. We do not find the increase in spreading with increasing beam energy as reported by them, although altitude profiles of energy deposition are the same. As an example, we predict ~½ as much spreading at a starting beam electron energy of 20 keV.

The spreading of e beams is a subject of considerable interest following the many rocket e beam experiments over the past decade (see review by *Winckler* [1980]) and planned experiments from both rockets and orbital vehicles. Much of this interest focuses on the importance of wave-particle effects in spreading beams beyond their widths produced by particle-particle effects alone, i.e., by multiple scattering and energy loss due to the neutral particle background. There is evidence from the past experiments that wave-particle effects can, in fact, be disruptive to the beam. Perhaps the most obvious case comes from ECHO IV where some optically measured streaks are diffuse, while others appear sharp [*Hallinan et al.*, 1978]. As much as a factor of 5 difference in widths is observed for streaks in these categories.

ANALYTIC MODEL AND DISCUSSION

The applied analytic model is based on the following physical description. An electron begins with energy E_o directed parallel to the magnetic field. Its distribution in pitch angle after N scatterings is given by the Goudsmit-Saunderson multiple scattering distribution. Energy loss is assumed to be continuous, given by the Bethe stopping power formula. Finally, the distribution of angles for any single scattering event is given by a screened Rutherford formula. The model may be conveniently divided into two parts. One part shows that the radial aspect of the electron transport can be represented by two-dimensional random walking of the guiding center (GC). The key parameter to come from this part is l_i the average GC displacement in the x-y plane (perpendicular to B) caused by the ith collision. The other part of the model applies the concept of random walking in two dimensions giving the GC radial distribution as a function of N, the number of scatterings. From this comes the quantity sought in this work, the average radius of the energy deposition. We choose to present this part of the model first, which leads us immediately to the results. The other part, some of it being of a geometric nature, is presented in Appendix A.

We begin with the guiding center located at $r = 0$. Upon the ith collision it makes an average displacement l_i in the x-y plane random in direction. To apply the GC distribution function below, l_i must be constant. Since we are interested in an approximate upper bound to the spreading caused by particle-particle effects, l_i, which is a slowly varying function of i, is replaced by l_o, an upper bound to l_i (see Appendix A). The needed probability distribution can now be expressed by

$$W_N(r) = (\pi N l_o^2)^{-1} \exp\left(-\frac{r^2}{N l_o^2}\right) \qquad (1)$$

with normalization given by

$$\int_0^\infty W_N(r) 2\pi r \, dr = 1 \qquad (2)$$

Equation (2) is the two-dimensional random walk distribution applicable to $N \gg 1$ and follows from the three-dimensional expression given by *Chandrasekhar* [1943]. We see that the distribution becomes flatter and wider as the number of scatterings increases. The average radius of the particle distribu-

---

[1] Present address is Bell Laboratories, Holmdel, New Jersey 07733.

tion after N scatterings, $\langle r_N \rangle$, is

$$\langle r_N \rangle = (\pi N)^{1/2} \frac{l_o}{2} \qquad (3)$$

In our model, energy loss is continuous along the electron trajectory, which provides a sound description for energies of interest, i.e., keV energies. Thus, between scatterings the electron deposits energy uniformly on a radius r_g (electron gyroradius) centered about the given guiding center. Let us assume that this deposition takes place at the guiding center. Then the distribution for energy deposition is given by

$$D(r) = \sum_{i=1}^{N_o} \Delta E_i W_i(r) \quad \text{eV/unit area} \qquad (4)$$

where N_o is the number of scatterings corresponding to total energy loss. The average radius of energy deposition $\langle r \rangle_D$ is

$$\langle r \rangle_D \simeq 1 + \frac{\sqrt{\pi}}{2} l_o \sum_{i=1}^{N_o} \frac{\Delta E_i}{E_o} \sqrt{i} \qquad (5)$$

where the sum comes from use of (4) and W_i is given by (1). The unit length is taken to be the gyroradius v_o/ω, where v_o and ω are the initial speed and gyrofrequency. W_i is not accurate for small i, and, in turn, the first several summed terms in (5) are not accurate. This will not produce significant error, however, because of the large size of N_o. The unit term above accounts for deposition taking place a gyroradius from the guiding center.

We can cast $\langle r_D \rangle$ into a more usable form noting that ΔE_i is slowly varying and can thus be removed from the summation in its averaged form (see Appendix B). We now have

$$\langle r \rangle_D \simeq 1 + \frac{\sqrt{\pi}}{2} l_o \frac{\overline{\Delta E}}{E_o} \sum_{i=1}^{E_o/\overline{\Delta E}} \sqrt{i} \qquad (6)$$

Since the number of scatterings $N = E_o/\overline{\Delta E}$ is large, we may take the continuum limit, giving

$$\langle r \rangle_D \simeq 1 + \frac{\sqrt{\pi}}{2} l_o \frac{\overline{\Delta E}}{E_o} \frac{2}{3} \left(\frac{E_o}{\overline{\Delta E}} \right)^{3/2}$$

$$\simeq 1 + \frac{1}{3} \sqrt{\pi} l_o \left(\frac{E_o}{\overline{\Delta E}} \right)^{1/2} \qquad (7)$$

Inserting the expressions for $\overline{\Delta E}$, l_o, and η_o from the appendices, we arrive at the desired form:

$$\langle r \rangle_D \simeq 1 + \frac{1}{3} \left(\frac{\pi Z}{2} \right)^{1/2} \left(\frac{\ln E_o/E_s - 2}{\ln E_o/I - 1} \right)^{1/2} \qquad (8)$$

It is worth noting the simple physics revealed by this equation. The numerator inside the last square root represents scattering, while the denominator represents energy loss. If either is set to zero, which corresponds to turning off that mechanism, $\langle r \rangle_D$ gives the expected result. The actual value of the square root quantity will be near unity for our applications, and thus the average radius for energy deposition is about two initial gyroradii. This is shown in Figure 1 along with available observations for rocket e beam experiments. We note that our simple form for $\langle r \rangle_D$ provides reasonable agreement for beam injection at low altitudes. Expression (8) and our Monte Carlo results are independent of altitude, in contrast to the data. The spreading observed for higher injection altitudes is

presumably caused by a combination of particle-particle and wave-particle effects.

In summary, we have shown that the lateral spreading of an e beam by particle-particle interactions can be formulated as a two-dimensional random walk problem involving the electron guiding center. Applying the concept of random walking, a simple expression is derived for the average radius of energy deposition for an initially monoenergetic, field-aligned e beam. This expression should overestimate rather than underestimate the beam spreading, although not by much. The overestimate is based on the use of l_o rather than l_i as the radial displacement per collision. Subsequent approximations that were made should not bias the results in a similar fashion. We find that the average radius of energy deposition is only about two initial gyroradii and, furthermore, is only weakly dependent on energy. The observed dependence in spreading is in conflict with the Monte Carlo results of *Berger et al.* [1970] but is in good agreement with our own Monte Carlo results. We further observe generally good agreement with the e beam spreading measurements of *Hallinan et al.* [1978] for beam injection below ~160 km and with the Monte Carlo models of *McEntire* [1973] and *Halbleib* [1974].

APPENDIX A: DERIVATION OF RADIAL DISPLACEMENT l_i

The concept of guiding center diffusion is introduced together with a derivation of the radial displacement of the guiding center per scattering. Use will be made of both multiple scattering and single scattering concepts. Consider an electron starting with energy E_o moving downward along a geomagnetic field line. As it proceeds, it loses energy and undergoes scatterings, thereby providing a perpendicular component to its velocity and, in turn, precession about some fixed guiding center between scatterings. Let v_i be the velocity just as the electron begins its ith elastic collision. In the $x - y$ plane the electron is positioned at (x_i, y_i), while its guiding center is at (x_g', y_g'). These coordinates are related by

$$x_g' = x_i - \frac{v_y'}{\omega} \qquad (A1)$$

and

$$y_g' = y_i + \frac{v_x'}{\omega} \qquad (A2)$$

where ω is the gyrofrequency.

The electron now undergoes its ith collision. While its position does not immediately change, its velocity vector does, and in turn, so does the position of the guiding center. We wish to know the relationship between the changes in these quantities. Let (v_i, Θ, Φ) be the spherical coordinates of v_i in a fixed frame with field $\mathbf{B}$ along z. Further, let θ and ϕ be the pitch and azimuthal scattering angles with respect to v_i. Then the change in v_i in terms of its components projected onto the $x - y$ plane, can be shown to be

$$\Delta v_x' = v_i[-\cos\Theta\cos\Phi\sin\theta\cos\phi + \sin\Phi\sin\theta\sin\phi$$
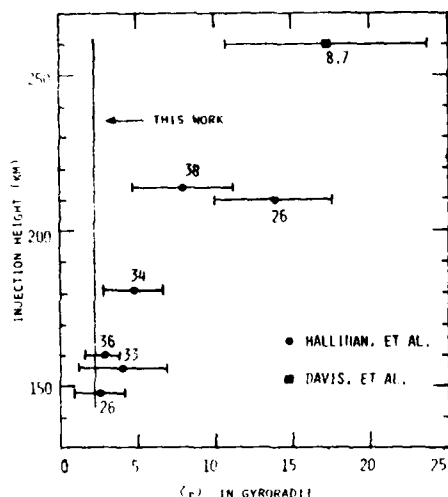$$+ \sin\Theta\cos\Phi(\cos\theta - 1)] \qquad (A3)$$

Fig. 1. Mean radius of energy deposition as a function of height for several streaks of different energies. Numbers above data points are beam energies in keV.

and

$$\Delta v_y' = v_i[-\cos\Theta\sin\Phi\sin\theta\cos\phi - \cos\Phi\sin\theta\sin\phi$$

$$+ \sin\Theta\sin\Phi(\cos\theta - 1)] \quad (A4)$$

Noting from (A1) and (A2) that

$$\Delta x_g' = -\frac{\Delta v_y'}{\omega} \quad (A5)$$

and

$$\Delta y_g' = \frac{\Delta v_x'}{\omega} \quad (A6)$$

we are now able to relate the GC radial displacement Δr_i to the change in velocity. In squared form, it is

$$\Delta r_i^2 = \frac{v_i^2}{\omega^2}[\cos^2\Theta\sin^2\theta\cos^2\phi$$

$$+ \sin^2\theta\sin^2\phi + \sin^2\Theta(\cos\theta - 1)^2$$

$$- \tfrac{1}{2}\sin 2\Theta\sin\theta\cos\phi(\cos\theta - 1)] \quad (A7)$$

We note that Δr_i^2 is independent of Φ, which introduces the randomness in radial motion of the guiding center that we are seeking.

To proceed, we must introduce the probabilistic nature of the problem, since the angles in (A7) can only be related to the ith scattering through probability distribution functions. Specifically, a multiple scattering distribution function governs the behavior of Θ, while a single scattering distribution function governs that of θ. A uniform distribution is assigned to ϕ due to the azimuthal symmetry of the single scattering process. Let $p_i(\cos\Theta)$ and $f_i(\cos\theta)$ be the multiple and single scattering distributions. We use for p_i a generalization of the *Goudsmit and Saunderson* [1940] formula, which is

$$p_i(\cos\Theta) = \frac{1}{4\pi}\sum_{l=0}^{\infty}(2l+1)\prod_{j=1}^{i-1}\langle P_l(\cos\theta)\rangle_j P_l(\cos\Theta) \quad i > 1$$

$$(A8)$$

where the averaged Legendre polynomial is

$$\langle P_l(\cos\theta)\rangle_j = \frac{\int P_l(\cos\theta)f_j(\cos\theta)\,d\cos\theta}{\int f_j(\cos\theta)\,d\cos\theta} \quad (A9)$$

For the single scattering distribution f_j we use

$$f_j(\cos\theta) = f(E_j,\cos\theta) = \frac{\eta_j(1+\eta_j)}{\pi}\frac{1}{(1-\cos\theta+2\eta_j)^2} \quad (A10)$$

with screening parameter η_j given by

$$\eta_j = \left(\frac{Z^{1/3}}{0.885}\right)^2\frac{me^4}{\hbar^2}\frac{1}{8E_j} \quad (A11)$$

Expression (A10) with this form of η_j comes from use of a Thomas-Fermi model with exponential screening by the bound electrons. We equate E_s with the constant terms in (A11), giving

$$\eta_j = E_s/E_j \quad (A12)$$

E_s appeared explicitly in the key quantity derived in this paper, $\langle r\rangle_D$, and thus for the convenience of the reader we note its form as a function of Z:

$$E_s = 4.3Z^{2/3}\quad\text{eV} \quad (A13)$$

Returning to p_i and f_i, their normalizations are

$$\int p_i(\cos\Theta)\,2\pi\,d\cos\Theta = 1 \quad (A14)$$

and

$$\int f_i(\cos\theta)\,2\pi\,d\cos\theta = 1 \quad (A15)$$

The probability density function for the ith step to have step size can now be given. It is

$$\tau_i(r) = 2\int p_i(\cos\Theta)f_i(\cos\theta)\,\delta(r^2 - \Delta r_i^2)\,d\phi\,d\cos\theta\,d\cos\Theta \quad (A16)$$

where the delta function provides the necessary restrictions on integrations limits such that any given combination of angular values gives only r. The normalization on τ is

$$2\pi\int\tau_i(r)r\,dr = 1 \quad (A17)$$

In the main text we introduced the average guiding center displacement for the ith collision l_i. To apply the given two-dimensional random walk model, l_i was replaced by l_o, its value at the starting energy. There we noted that l_o provided an upper bound to l_i. We now give the form of l_i (in squared form) from which it will be clear that l_o is its maximum value. It is the average value of Δr_i^2 and is thus given by

$$l_i^2 = 2\pi\int r^2\tau_i(r)r\,dr$$

$$= 2\pi\int\Delta r_i^2\,p_i(\cos\Theta)f_i(\cos\theta)\,d\cos\Theta\,d\cos\theta\,d\phi \quad (A18)$$

In gyroradius units referenced to $E_0(v_0/\omega)$ this becomes

$$l_i^2 = \frac{E_i}{E_0}(\sin^2\theta)_i\frac{(1+\cos^2\Theta)_i}{2} \quad (A19)$$

where the $\langle(\cos\theta - 1)^2\rangle_i$ term in Δr_i^2 has been dropped. Its contribution can be ignored for kilovolt electrons due to f_i being so strongly forward peaked. The quantity l_i^2 is slowly decreasing, as can be demonstrated by noting the form of

$\langle \sin^2 \theta \rangle_i$. For the given f_n, it can be shown to be

$$\langle \sin^2 \theta \rangle_i = 4\eta_i(|\ln \eta_i| - 2) \tag{A20}$$

Since $\eta_i E_i$ is constant, the first part of (A19), i.e., $E_i/E_0 \langle \sin^2 \theta \rangle_i$ varies as $|\ln \eta_i| - 2$. This is a decreasing function of i, since η_i is increasing from a starting value of about 10^{-4}. It is clear that $\langle 1 + \cos^2 \Theta \rangle_i$ decreases from a starting value of 2. Its actual variation for the given p_i is

$$\langle 1 + \cos^2 \Theta \rangle_i = \left\{ 4 + 2 \prod_{j=1}^{i-1} \langle P_j(\cos \theta) \rangle_j \right\} \bigg/ 3 \quad i > 1 \tag{A21}$$

The explicit form of l_o^2 based on the above considerations is

$$l_o^2 = 4\eta_o(|\ln \eta_o| - 2) \tag{A22}$$

APPENDIX B: DERIVATION OF THE AVERAGE ENERGY LOSS PER COLLISION $\overline{\Delta E}$

In this appendix, we given the forms of ΔE_i and its averaged value $\overline{\Delta E}$. It will be shown that ΔE_i is slowly varying, which allows it to be replaced by $\overline{\Delta E}$ in (5) without introducing significant error. ΔE_i is defined as the energy loss per collision, i.e., loss over an elastic mean free path at the ith scattering. In the continuous energy loss approximation applied to this work its form is

$$\Delta E_i = \frac{8E_i}{Z} \eta_i \ln \frac{E_i}{I} \tag{B1}$$

which comes from $(dE/dx)\Delta s_i$, where dE/dx, the stopping power, is given by the Bethe formula,

$$\frac{dE}{dx} = \frac{4\pi n Z}{m v^2} e^4 \ln \frac{E}{I} \tag{B2}$$

and Δs_i, the mean free path between scatterings, is

$$s_i = \frac{p^2 v^2 \eta_i}{n Z^2 e^4 \pi} \tag{B3}$$

The energy parameter I appears explicitly in our final expression for $\langle r \rangle_D$ (equation (8)) and has the form

$$I = 9.1Z(1 + 1.9X^{-2/3}) \tag{B4}$$

[Segre, 1964]. We observe that ΔE_i has only logarithmetic energy dependence, since $E_i\eta_i = E_S$ (see Appendix A). To obtain $\overline{\Delta E}$, we may thus apply the continuum limit, giving

$$\overline{\Delta E} = \frac{8E_S}{Z} \left[\ln \frac{E_o}{I} - 1 \right] \tag{B5}$$

REFERENCES

Berger, M. J., S. M. Seltzer, and K. Maeda, Energy deposition by auroral electrons in the atmosphere, *J. Atmos. Terr. Phys., 32,* 1015, 1970.

Chandrasekhar, S., Stochastic problems in physics and astronomy, *Rev. Mod. Phys., 15,* 1, 1943.

Davis, T. H., T. J. Hallinan, G. D. Mead, J. M. Mead, M. C. Trichel, and W. N. Hess, Artificial aurora experiment: Ground-based optical observations, *J. Geophys. Res., 76,* 6082, 1971.

Goudsmit, S., and J. L. Saunderson, Multiple scattering of electrons, *Phys. Rev., 57,* 24, 1940.

Halbleib, J. A., Sr., Electron transport in the presence of uniform magnetic fields, *IEEE Trans. Nucl. Sci., 21,* 221, 1974.

Hallinan, T. J., H. C. Stenback-Nielsen, and J. R. Winckler, The ECHO IV electron beam experiment: Television observation of artificial auroral streaks indicating strong beam interactions in the high-latitude magnetosphere, *J. Geophys. Res., 83,* 3263, 1978.

McEntire, R. A., The electron ECHO experiment: A comparison between the observed and predicted trajectories of electrons artificially injected into the magnetosphere, Ph.D. thesis, Univ. of Minn., Minneapolis, 1973.

Segre, E., *Nuclei and Particles,* Benjamin, New York, 1964.

Winckler, J. R., The application of artificial electron beams to magnetospheric research, *Rev. Geophys. Space Phys., 18,* 659, 1980.

DA
FILM